Survival of Archean cratonal lithosphere

Norman H. Sleep
Department of Geophysics, Stanford University, Stanford, California, USA

Received 23 January 2001; revised 13 December 2002; accepted 30 December 2002; published 17 June 2003.

[1] I use thermal convection models to search for combinations of physical parameters that are compatible with the results of xenolith studies on the history and present thermal structure of cratonal lithosphere. The cratonal lithosphere above ~180 km depth formed in the Archean and remained stable until recently sampled. The mantle adiabat cooled ~150 K over this time. The temperature change across the rheologically active boundary layer at the lithospheric base is <300 K over a depth range of several tens of kilometers. Modern cratonal lithospheric thicknesses are relatively uniform, ~225 km, much thicker than old oceanic lithosphere. Cratonal lithosphere is now in quasi-steady state with conductive heat flow to the surface in balance with heat supplied to the base of the lithosphere by convection driven by local temperature contrasts within the rheologically active boundary layer. This heat flow and the lithosphere thickness changed little after the cratonal lithosphere stabilized. One possibility is that chemically buoyant lithosphere forms a conductive lid above the convecting normal mantle. To survive, the chemical lithosphere also needs to be more viscous than normal mantle. A reasonable situation has chemical lithosphere a factor of 20 more viscous than normal mantle with weakly temperature-dependent viscosity (a factor of e over 100 K) from 0.2×10^{20} Pa s along the modern mantle adiabat. However, a chemical lid is unnecessary for lithospheric thickness to change slowly over time. For example, the base of the lithosphere may be stable if the viscosity at its base (along an adiabat) decreases rapidly with depth. *INDEX TERMS:* 8120 Tectonophysics: Dynamics of lithosphere and mantle—general; 8121 Tectonophysics: Dynamics, convection currents and mantle plumes; 8125 Tectonophysics: Evolution of the Earth; 8159 Tectonophysics: Rheology—crust and lithosphere; *KEYWORDS:* craton, lithosphere, entrainment, heat flow, convection

Citation: Sleep, N. H., Survival of Archean cratonal lithosphere, *J. Geophys. Res.*, *108*(B6), 2302, doi:10.1029/2001JB000169, 2003.

1. Introduction

[2] Cratonal regions of the Earth's continents are defined by their lack of geological activity. This prolonged quiescence is a marked contrast to the ocean basins where the crust and lithosphere are less than 200 Ma and to the active regions of the continents. The salient features of cratons are stability often over the last 2–3 Gyr, lithosphere over 200 km thick, and often exposure of Precambrian rocks over large regions.

[3] Basic physical aspects of the stability of cratons are well known. The buoyancy of the continental crust, in general, and any chemical buoyancy in the underlying continental mantle resist subduction [e.g., *Bickle*, 1986; *Pollack*, 1986; *Abbott et al.*, 1997]. The lithosphere tends to fail so that strain concentrates along faults that form preferentially within thin lithosphere. This causes most plate tectonic deformation to occur outside of cratons [e.g., *Moresi and Solomatov*, 1998; *Lenardic et al.*, 2000].

[4] Recent studies of xenolith data summarized in section 2.1 define the modern geotherm in the mantle lithosphere beneath cratons [*Rudnick and Nyblade*, 1999]. The base of the lithosphere is within a narrow depth range between 200 and 250 km. In addition, osmium isotopic ages from cratonal xenoliths are Archean [*Carlson et al.*, 1999; *Pearson*, 1999]. The straightforward, but not unique, interpretation is that much of the Archean cratonal lithosphere was emplaced and stabilized in the Archean and has not changed significantly since then. This inference is explicit in recent petrological interpretations of xenoliths [*Hanghøj et al.*, 2001; *Saltzer et al.*, 2001].

[5] The purpose of this paper is to study the persistence of cratonal lithosphere as a heat and mass transfer problem. That is, cratonal lithosphere is significantly thicker than old oceanic lithosphere, yet much thinner than it would be if it had simply cooled from above by conduction since the Archean. The thermal implication of the xenolith studies is that cratonal lithosphere approached its present thickness soon after the cratons stabilized. Since then, the base of the craton has been approximately steady state with the heat supplied to the lithosphere from the rest of the mantle balancing the heat that flows upward to the surface.

[6] This problem is distinct from the more difficult problem of how cratonal lithosphere formed in the first place. Archean cratons are temporally and spatially complex

0148-0227/03/2001JB000169$09.00

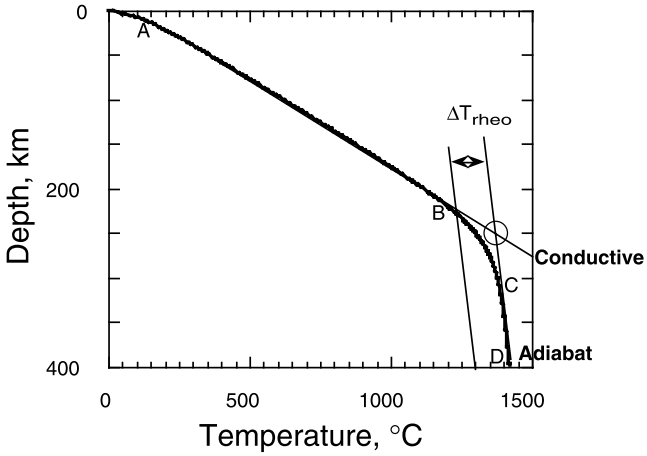

Figure 1. Schematic diagram of the geotherm beneath a craton. The geothermal gradient is conductive in the rigid lithosphere between A and B. The geotherm is curved in the rheologically active boundary layer between B and C and adiabatic between C and D. The potential temperature contrast across the rheologically active boundary layer is T_{rheo}. The intersection of the extrapolated conductive geotherm with the extrapolated adiabat is a convenient scale depth and temperature for the base of the lithosphere.

like the products of modern plate tectonics. Clearly, the formation mechanism of cratonal lithosphere cannot be incompatible with its longevity. Beyond that, I do not attempt to constrain how cratonal lithosphere formed.

2. Observational Evidence and Constraints

[7] I begin with the geotherm within and beneath the cratonal lithosphere (Figure 1). At shallow depths, the lithosphere is rigid; heat flows by conduction (segment A-B, Figure 1). A rheologically active thermal boundary layer exists near the base of the lithosphere (segment B-C, Figure 1). Conduction and convection both transfer heat within this region. The region beneath the thermal boundary layer convects and is essentially adiabatic (segment C-D, Figure 1). Xenolith data confirm this arrangement [*Rudnick and Nyblade*, 1999]. However, uncertainties in xenolith pressure and temperature obscure the details of the geotherm within the thermal boundary layer at the base of the lithosphere. In addition, the studied magmas carried no xenoliths from the adiabatic region beneath the boundary layer, probably because the source regions of the magmas were shallower than this region.

[8] The depth to a particular isotherm does not usefully define the base of the lithosphere, in part, because the Earth's interior cools with time [*Grasset and Parmentier*, 1998]. In addition, different geophysical and geological methods sense different features of the transition from lithosphere to adiabatic mantle and yield different estimates of the lithospheric base. These potentially observable details of the lithospheric base are not now well resolved.

[9] Cratonal lithosphere is likely to be chemically buoyant with respect to normal mantle. Such buoyancy clearly aided the initial stabilization of cratons within the convecting Earth. It may also be relevant to the longevity of cratonal lithosphere. In that case, the chemical lithosphere needs to extend downward into the rheologically active boundary layer so that its buoyancy affects flow. Then the interface at the base of the buoyant region was a quasi-stable lid to the underlying convection. Convective downwellings entrained the chemical lithosphere into cusps, which resisted further downwelling. Lithospheric thickness changed slowly as buoyant material was gradually entrained into the normal mantle and the vigor of convection changed as the Earth's interior cooled [*Jordan*, 1981; *Richter*, 1988; *Doin et al.*, 1997; *Shapiro et al.*, 1999a].

[10] Much geological and geophysical data relate to the temperature and chemical buoyancy of cratonal lithosphere. I start with xenolith data in section 2.1, which supply the most reliable information on the modern geotherm, the age of cratonal stabilization, and the thickness of the rheologically active boundary layer. I continue with other methods for constraining the geotherm in section 2.2. Until recently, heat flow and seismology supplied most of the information on modern cratonal structure. Intraplate stress and geoid provide the best information on the existence of chemically buoyant lithosphere and some information on the modern and the ancient cratonal geotherm. I consider constraints on mantle viscosity in section 2.3, a topic that is important to heat and mass transfer within the rheologically active boundary layer.

2.1. Evidence From Xenoliths and Magmas

[11] The geotherm in the past (as well at the present) is constrained by considering the nature (or lack of) lithosphere-derived melts and by studying xenoliths erupted through the craton in lavas of various ages. An early example of the former method uses the observation that volcanism from melting of the base of continental crust did not occur continually in the Archean (nor later in Earth history) [*Burke and Kidd*, 1978]. This indicates the base of the Archean crust was typically too cold to melt and substantially cooler than the Archean mantle adiabat. That is, the Archean lithosphere was already significantly thicker than the crust. Modern xenolith data confirm this inference and provide far more detailed information.

[12] Suites of cratonal xenoliths directly yield the modern geotherm at the time of eruption [*Rudnick and Nyblade*, 1999]. The slope of the conductive part of the geotherm within the rigid lithosphere is well resolved (Figure 1). This yields conductive heat flows through the lithosphere between 17 and 25 mW m^{-2}. The studies constrain the depth to the base of the lithosphere and the geotherm within the rheologically active boundary layer. There are no sampled xenoliths to constrain the geotherm beneath the rheologically active boundary layer. The deepest xenoliths come from a depth 200–250 km for the South Africa, Slave, Superior, and Siberian cratons. The greatest depth in the Fennoscandian shield is ~240 km [*Kukkonen and Peltonen*, 1999]. The geotherm from the xenolith suite intersects the mantle adiabat in this depth range.

[13] The fabric of the deeper xenoliths provides direct evidence of an actively deforming rheological boundary layer [*Rudnick and Nyblade*, 1999]. Xenoliths from shallow depths have slowly recrystallized and show a nonsheared fabric. Deeper xenoliths are strongly sheared showing recent deformation. The transition depth is ~180 km

beneath South Africa [*Saltzer et al.*, 2001]. The temperature range across the rheological boundary layer from both the sheared xenoliths and the curvature of the geotherm is less than few hundred kelvins. The depths and temperatures determined by *Rudnick and Nyblade* [1999] indicate that sheared xenoliths were above ~1000°C or within ~300 K of the mantle adiabat.

[14] The xenolith studies provide an additional demanding constraint that the lithosphere quickly approached its presence thickness once it stabilized and remained stable since then. A 150- to 200-km-thick lithosphere beneath South Africa in the Archean is implied by Archean age diamonds [*Boyd et al.*, 1985]. Osmium isotopic studies of worldwide xenoliths indicate that the lithosphere above 150–200 km has remained stable over at least the last 2 Gyr [*Carlson et al.*, 1999; *Pearson*, 1999]. The dated xenoliths are the products of metasomatism, rather than pristine high-Mg residua from extensive partial melting (which are unsuitable for the Os method). The xenolith data indicate that age boundaries within the craton have persisted down to at least 200 km. The cratonal lithosphere has not been totally inactive as some younger xenoliths exist. The ages of rocks correlate with those of intense magmatic activity at the surface. This indicates that episodic events, as might be associated with underplating of a craton by plume material rather than gradual convective replacement of the base of the lithosphere, occurred. The laterally narrow Tanzania craton above 140 km depth has remained stable [*Chesley et al.*, 1999]. Somerset Island at the edge of the Canadian shield has remained stable down to 150 km where the rocks are now 1100°C [*Schmidberger et al.*, 2002].

[15] The straightforward inference from the xenolith data is that Archean rocks preserve an in-place record of Archean processes [e.g., *Saltzer et al.*, 2001; *Hanghøj et al.*, 2001; *Schmidberger et al.*, 2002]. For example, the South African xenoliths studied by *Saltzer et al.* [2001] indicate that Archean exosolution features above ~180 km depth have not been subsequently sheared and thus not entered the rheologically active boundary layer.

[16] Cratonal xenoliths are often highly depleted and contain very Mg-rich olivine and orthopyroxene. The processes that formed the xenoliths are variable, complex, and not fully understood. Source region temperatures of a few hundred kelvins greater than modern mid-ocean ridge basalt source temperatures were needed to form certain highly depleted mantle rocks found in xenolith suites [*Herzberg*, 1999]. This temperature is greater than the estimated temperature of normal Archean mantle, ~150 K greater than present [*Abbott et al.*, 1994]. *Saltzer et al.* [2001] conclude that their xenoliths formed above a subducting slab. *Hanghøj et al.* [2001] conclude that some of their xenoliths were formed by high degrees of polybaric melting and then were metasomatized. *Haggerty and Sautter* [1990] conclude that some xenoliths first equilibrated at ~400 km before becoming part of the lithosphere at ~180 km depth. *Macdougall and Haggerty* [1999] further show that the mantle source regions of some xenoliths ascended and became part of the lithosphere in modern times. Mantle plumes associated with kimberlite volcanism are the likely source of this material.

[17] Whatever processes that formed cratonal mantle, it is obvious that continental crust is not, on average, the komatiitic melts which were extracted to deplete mantle xenoliths [*Herzberg*, 1999]. This indicates prolonged processes formed continental crust, especially since a significant fraction of the Earth's highly incompatible elements, like U, Th, and K, ended up in the crust. That is, vast amounts of mantle recycled through the melting zone beneath cratonal crust before it stabilized. The ascending mantle and the depleted residuum had to deform and flow for this to occur. The lithosphere deformed to accommodate the source regions of modern plume-related xenoliths studied by *Macdougall and Haggerty* [1999]. I assume, however, that the net addition of plume-related material to the cratonal lithosphere over its later history is small and do not include this process in my modeling. Smaller cratons, such has North China, have lost their Archean lithospheric roots, probably by low-angle subduction [*Gao et al.*, 2002]. I do not attempt to constrain lithospheric rheology using these processes beyond noting that it did deform at various times.

2.2. Other Geophysical Constraints on Cratonal Thickness

[18] I review the implications of heat flow, seismic, and geoid studies to cratonal thicknesses. These lines of evidence are overall compatible with my inferences from xenoliths less robust.

2.2.1. Heat Flow Studies

[19] The great age of cratons allows heat flow data to be modeled as quasi-steady state conduction through a rigid lithosphere (Appendix A). One measures heat flow in shallow boreholes and mines at various places. One estimates the mantle heat flow into the base of the crust as follows [e.g., *Jaupart and Mareschal*, 1999; *Artemieva and Mooney*, 2001]. The measured heat flow is the sum of the contribution of heat flow coming into the base of the crust and heat generated within the crust by radioactivity. One obtains the mantle heat flow by subtracting estimates of the crustal radioactive terms from the surface heat flow. *Jaupart et al.* [1998], for example, compile mantle heat flows of 7–15 mW m^{-2} for the Canadian shield. *Jaupart and Mareschal* [1999] obtain 10–15 mW m^{-2} for eastern Canada and 17 mW m^{-2} for the Kaapvaal craton. *Artemieva and Mooney* [2001] obtain ~20 mW m^{-2} for the Canadian shield, ~10 mW m^{-2} for West Africa, and ~13 mW m^{-2} for parts of Siberia. It is not clear how much of this variation is real and how much results from errors in estimates of crustal radioactive heat generation.

[20] One obtains the lithospheric geotherm by extrapolating the temperature downward assuming conduction. The estimated lithospheric thickness is the depth that the estimated conductive geotherm intersects the mantle adiabat (Figure 1). In contrast with the xenolith data, heat flow estimates of lithospheric thickness are highly variable with West Africa and Siberia >350 km and the Canadian shield ~200 km [*Artemieva and Mooney*, 2001]. This range may be the unstable result of subtracting two comparable numbers to get mantle heat flow and dividing by this number to get lithospheric thickness.

2.2.2. Seismic and Magnetotelluric Lithosphere Thickness

[21] Seismic studies of deep cratonal lithosphere now have enough resolution to be useful [e.g., *Anderson and Polet*, 1995; *van der Lee and Nolet*, 1997; *Röhm et al.*,

2000]. Detailed local studies exist for some areas [e.g., *Bank et al.*, 1998; *Ritsema et al.*, 1998; *Simons et al.*, 1999; *Priestley*, 1999; *Ritsema and van Heist*, 2000]. The more reliable studies take explicit account of downward smearing of cratonal features, a well-known artifact of tomographic inversion. The depth ~230 km, where tomographic velocity anomalies approach resolution and cease to correlate which surface features, is a robust measure of seismic lithospheric thickness [*Röhm et al.*, 2000]. It is shallower than 250 km in the studies by *Simons et al.* [1999] and by *Ritsema and van Heist* [2000].

[22] Magnetotelluric studies are sensitive to water, a trace constituent in the mantle, which may significantly affect viscosity. The lithospheric mantle of Archean age currently contains less water than normal mantle between ~150 and ~250 km depth [*Hirth et al.*, 2000]. Cratonal mantle below ~250 km does not differ from normal mantle. These data provide little detail on the transition zone between lithosphere and asthenosphere.

2.2.3. Geoid and Intraplate Stress

[23] The low chemical density of continental lithosphere relative to the mantle beneath ridge axes produces positive geoid anomalies and horizontal lithospheric tension. The colder dense lithosphere of the continents produces negative geoid elevation and horizontal compression. Geoid measurements thus constrain the modern thermal and chemical structure beneath cratons. Tectonic features constrained this structure in the past. In particular, dikes and grabens indicate horizontal extension, while reverse faults indicate horizontal compression.

[24] I quantify these effects using isostasy. I separate the effects of chemical heterogeneity from those of temperature. The elevation of a continental region above ridge axes in linearized form is

$$E = \left[\frac{\rho_m}{\rho_m - \rho_w}\right] \int \left[\frac{\Delta\rho_C}{\rho_m} - \frac{\rho_{\mathrm{ref}}\alpha\Delta T_C}{\rho_m}\right] dz, \qquad (1)$$

where ρ_m is the density of the mantle compensating layer, ρ_w is the density of ocean water, $\Delta\rho_C$ is the chemical density deficit continental lithosphere (including the crust) relative to oceanic lithosphere, ρ_{ref} is a reference density, g is the acceleration of gravity, α is the volume thermal expansion coefficient, ΔT_C is the temperature of continental lithosphere below that of an adiabat at the ridge axis, and z is depth. (Both ρ_{ref} and α may be functions of depth; only their product enters into the final result.) The integral extends from the surface down to a depth where the mantle is basically adiabatic. The first term in brackets corrects for the load of the water filling the ocean basin; it is 1 for topography above sea level that is adjacent to air with negligible density. The $\Delta\rho_C$ term for the chemical buoyancy of continental crust and mantle produces positive elevation which is greater than the negative elevation from the ΔT_C term for the cold continental geotherm so that continents are typically higher than ridge axes.

[25] The geoid height H and the intraplate stress resultant (in units of stress per length) F are proportional to the integral of density contrast times depth:

$$H \propto F \propto \int \left[\frac{\Delta\rho_C}{\rho_m} - \frac{\rho_{\mathrm{ref}}\alpha\Delta T_C}{\rho_m}\right] z dz, \qquad (2)$$

where both quantities are relative to those at the ridge axis. The actual intraplate stress resultant is approximately that in equation (2) as little deviatoric stress is expected to be present beneath the ridge axis. Topography, geoid, and stress have poor resolution as these quantities depend on integrals of density throughout the lithosphere.

[26] At present, stable North America and all other large cratons are under horizontal compression [*Zoback and Zoback*, 1997]. However, past episodes of dike intrusion and rifting indicate periods of at least regional horizontal extension. That is, buoyant plume material ponded beneath the lithosphere (through F in equation (2)) and stress concentrations associated with nearby plate boundaries were sometimes able to bring cratons into horizontal extension. The force to form thickened continental crust in the first place, which scales with the variation in F across oceanic plates, does not seem to have changed greatly since the Archean [*England and Bickle*, 1984].

[27] Overall, the constraint from elevation in equation (1) is that the freeboard of cratons has not changed much with time. Cratons have neither been systematically uplifted and deeply eroded nor have they systematically subsided and been deeply buried by sediments [e.g., *Galer and Mezger*, 1998]. The constraint from intraplate stress is similar in that compressional and tensional tectonics have both occurred and that no systematic trend is evident. Both these lines of evidence indicate that the density and temperature structure of cratonal lithosphere in equations (1) and (2) have not changed much since the time of their stabilization. This supports the conclusion drawn from xenolith data that cratonal lithosphere approached its present thickness a long time ago. Further quantification, which is not attempted in this paper, would require a sophisticated treatment of the effects of plate tectonics, plumes, and lower mantle density structure on geoid, elevation, and plate stresses [see *Forte and Perry*, 2000].

2.3. Mantle Viscosity Structure

[28] An acceptable explanation for the thermal state of cratons should be compatible with what is known about the modern viscosity structure of the mantle [*Doin et al.*, 1997]. That is, the heat and mass transfer near the base on the lithosphere depends on the viscosity structure of the upper mantle. I discuss some lines of evidence, which (if the mantle acts as a nonlinear fluid) give the apparent viscosity of arising from the stress state associated with mantle flow. I distinguish between the variation of viscosity along an adiabat from the actual variation of viscosity with depth, which depends on the local geotherm.

2.3.1. Constraints From Geodynamic Modeling

[29] Analyses of glacial rebound, of geoid anomalies, such as those associated with slabs, and of the deflection of mantle plumes by flow in the mantle provide constraints on the viscosity of the upper few hundred kilometers of the Earth. However, most glacial rebound studies provide little information about the viscosity near the base of the lithosphere. In particular, the existence of a low-viscosity zone between the base of the lithosphere and ~230 km depth is compatible with (but not required by) these data. *Pari and Peltier* [1998] and *Panasyuk and Hager* [2000] come to the similar conclusion from the analysis of geoid and tomography data. Details of shallow mantle structure are also not

obtained from studies of the deflection of plumes by flow in the mantle [*Steinberger and O'Connell*, 1998]. *Forte and Perry* [2000] and *Forte and Mitrovica* [2001], however, find a pronounced viscosity minimum in the seismic low-viscosity zone using combined tomographic and geodynamic models. *Richards et al.* [2002] point out that a shallow low-viscosity zone enhances plate-like behavior.

[30] In addition, the viscosity near the base of plates is potentially obtained from force balances. I illustrate the rudiments of the method and obtain crude estimates by considering the ridge-push force.

[31] The lithosphere is thin enough near fast ridge axes to be represented as a thin rigid sheet over adiabatic mantle. The observation that intraplate earthquakes in old oceanic crust indicate horizontal compression limits the shear stress from drag on fast moving plates [*Stein and Pelayo*, 1991]. Crudely, ridge push puts the plates into compression by being greater than the drag force at their bases. If the drag force were higher, the plates would have to be pulled by slabs putting them in tension. The qualitative scaling implied by this approach is valid even though neither plate-driving forces nor intraplate earthquakes are fully understood.

[32] The quantification of this effect follows *Stein and Pelayo* [1991]. An integral in the form of equation (2) gives the ridge push force for a cooling half-space. Retaining only the first-order term in equation (6–376) of *Turcotte and Schubert* [1982], the ridge push force acting on the plate is

$$F_R = \rho g \alpha T_H \kappa t_A, \tag{3}$$

where t_A is plate age, T_H is the half-space temperature beneath the lithosphere, and κ is thermal diffusivity. In the case that the plate is neither under compression nor tension, this force is balanced by drag acting over the base of the plate

$$F_D = V_{\text{plate}} t_A \tau_D, \tag{4}$$

where V_{plate} is the plate velocity, and $V_{\text{plate}} t_A$ is the width of the base of the plate over which the shear traction τ_D acts. To obtain a closed-form result, I represent a low-viscosity asthenospheric zone beneath the lithosphere as a channel of thickness Z_A and uniform viscosity η_A. Then the drag is

$$\tau_D = V_{\text{plate}} \eta_A / Z_A. \tag{5}$$

[33] Balancing for the forces in equations (3) and (4) and applying equation (5) yields the maximum value of the drag coefficient for which the plate can be under compression

$$\frac{\eta_A}{Z_A} = \frac{\rho g \alpha T_H \kappa}{V_{\text{plate}}^2}, \tag{6}$$

which is independent of the plate age t_A. For the assumed parameters, $t_A = 3400$ kg m^{-1}, $\alpha = 3 \times 10^{-5}$ K^{-1}, $\kappa = \sim 0.75 \times 10^{-6}$ m^2 s^{-1}, and a maximum plate velocity of 100 mm yr^{-1}, the drag coefficient is 10^{14} Pa s m^{-1} in agreement with *Stein and Pelayo* [1991]. For example, a 100-km-thick channel with a viscosity of 10^{19} Pa s produces this drag coefficient. This estimate should be adjusted upward somewhat if it is to apply to normal mantle. Hot low-viscosity plume material rather than normal mantle in part underlies the fastest moving plates in the South Pacific. In addition, the low viscosity of partially molten material beneath young lithosphere may lubricate the base of oceanic plates [*Tackley*, 2000].

[34] The same reasoning applies to cratons with even more uncertainty. As the typical cratonal velocity is a factor of $\sim 10^{1/2}$ less than fast oceanic plates, the upper limit on the drag coefficient for a linear fluid is a factor of ~ 10 greater than that for fast plate. Cratons also cover a modest fraction of their plate's total area so local regions with higher cratonal drag are permitted. This implies an upper limit for cratonal drag of a few 10×10^{14} Pa s m^{-1}. For a typical cratonal velocity, this implies maximum shear traction of a few megapascals.

2.3.2. Viscosity Parameterization

[35] There is at present no atomistic treatment that adequately represents the variation of viscosity with depth in the Earth. The viscosity of a single well-defined phase can be represented in terms of activation energies and volumes for each creep mechanism that occurs. However, the Earth's mantle is composed of several phases, and the phase assemblage and dominant creep mechanism may change gradually or rapidly with temperature and pressure. The base of the low seismic velocity zone between 200 and 250 km depth is an obvious candidate for the effects of depth-dependent phase change. That is, trace amounts of partial melt (or another weak grain boundary phase) that lower seismic velocity may also lower viscosity. The disappearance of these phases with depth then leads to an increase of viscosity with depth. Water, a trace constituent, may have significant effects on the viscosity of nominally anhydrous minerals, like olivine.

[36] The actual mantle viscosity is time-dependent at a given pressure and temperature because deformation reduces grain size while Ostwald ripening increases it [*Solomatov*, 2001]. It has not escaped me that this effect may aid to the stabilizing of very slowly deforming cratonal lithosphere. It is a potential means of quantifying of the transition between deep sheared xenoliths and shallow recrystallized ones in terms of strain rate. I ignore this topic for simplicity.

[37] I adopt an agnostic approach of representing temperature-, depth-, and chemical-dependent viscosity. Following *Doin et al.* [1997], I assume a function of the form

$$\eta = \eta_0 \left[\frac{\eta_C}{\eta_0}\right]^{\phi} \exp\left[\frac{\Delta T}{T_\eta}\right] \exp\left[\frac{z}{D_\eta}\right], \tag{7}$$

where η_0 is the viscosity of normal mantle at the surface and a reference adiabat, η_C is the viscosity of chemical lithosphere at the surface and reference temperature, z is depth, ΔT is temperature below that adiabat, T_η is the temperature scale to for viscosity, D_η is the depth scale, and the fraction of chemical lithosphere at a "point" in the mantle ϕ varies from 0 to 1. This formulation has the advantage that three easily understood parameters, η_0, T_η, and D_η, represent the behavior of ordinary mantle. Two parameters, η_C/η_0 and the chemical density contrast $\Delta\rho_C$, represent the contrast between ordinary and chemical lithosphere. I let the local chemical density contrast vary linearly as $\phi \Delta \rho_C$.

[38] The viscosity of the mantle may be nonlinear in the stress range of interest to mantle convection. The strain rate tensor in an isotropic material is then

$$\varepsilon'_{ij} = \frac{\tau_{ij}}{2\eta}\left[\frac{\tau}{\tau_{\mathrm{ref}}}\right]^{n-1}, \tag{8}$$

where τ_{ij} is the deviatoric stress tensor, η is the viscosity given by (7), τ is the square root of the second invariant of $\tau_{ij}\tau_{ij}$ normalized for convenience so that it yields the scalar shear traction in simple shear, τ_{ref} is a reference shear traction, and n is the power law exponent. This formation has the simplifying feature that all the depth and temperature dependence of rheology is included in the parameter η and that τ_{ref} may be chosen for convenience without loss of generality.

[39] My viscosity parameterization casts a wide net for models that satisfy observations. I present simple cases obtained from scaling arguments in sections 3.3 and 3.4. I do not attempt to cull the models with sophisticated mineral physics although the reader may wish to do so.

3. Heat and Mass Transfer Theory for Cratons

[40] I investigate heat and mass transfer beneath cratons. Qualitatively, Archean lithosphere approached its present thickness soon after it formed. The lithospheric material remained stable after that time until tiny amounts of it became xenoliths. Active deformation is currently occurring only within the source region of sheared xenoliths, that is, the rheologically active boundary layer. Younger platform lithosphere is almost as thick as Archean lithosphere even though its composition is different.

3.1. Parameterization of Observable Constraints

[41] To aid comparison of model predictions, I represent the observable properties of the lithosphere and its history with a few simple parameters. The reader can refine or even turn around my arguments when more becomes known from xenolithic and geophysical studies.

[42] I first parameterize the temperature and thickness of the lithosphere. I represent heat conduction within the lithosphere initially as a quasi-steady process where the heat flow is constant with depth (see Appendix A). I ignore the existence of the continental crust with its radioactivity and different conductivity. I also ignore the adiabatic gradient and use potential temperature. Then the quasi-steady heat flow is

$$q_H = k\frac{T_H}{Z_H}, \tag{9}$$

where the thermal conductivity k is constant (3 W m^{-1} K^{-1}), the conductive geotherm intersects the mantle adiabat at temperature T_H (relative to the surface temperature) and depth Z_H (Figure 1). Xenolith studies provide modern values of the lithospheric (scale) thickness Z_H. Studies of mid-ocean ridge basalts and xenoliths provide the modern mantle adiabat and the potential temperature T_H. It is currently $\sim$1300°C. For example, the heat flow is 17.5 mW m^{-2} for a lithospheric thickness of 220 km.

[43] The temperature range near the base of the lithosphere from which sheared xenoliths come yields an estimate temperature range ΔT_{rheo} across the rheological boundary layer. A second related estimate comes from the xenolith geotherm itself. That is, the geotherm is curved within the rheological boundary as the gradient decreases from the conductive gradient at the top of the layer to the adiabatic gradient at its base. Both lines of evidence from the xenolith arrays studied by *Rudnick and Nyblade* [1999] indicate that the temperature range across the boundary layer is <300 K. This is compatible with the results of *Schmidberger et al.* [2002], who found that rocks cooler than 1100°C have remained in place beneath Somerset Island, Canada.

[44] My selection of T_H, Z_H, and ΔT_{rheo} as lithospheric parameters has the advantage that none of them depend on the unresolved details of the geotherm where it intersects the adiabat. My best estimate for T_H is 1300°C and 225 km for Z_H. My upper limit for Z_H is 250 km. My upper limit for ΔT_{rheo} is 300 K. I do not attempt a best estimate or lower limit for ΔT_{rheo}.

[45] The change in lithosphere thickness since the Archean is another observable parameter. Xenolith data indicate that not much thickening has occurred. I obtain that the latest Archean lithosphere (as defined by the intersection of the adiabat with the conductive geotherm) was at least $\sim$200 km thick from the observation of *Saltzer et al.* [2001] that the lithosphere above 180 km has remained stable since then. That is, I leave $\sim$20 km for the part of the rheologically active boundary layer above 200 km depth. The Archean thickness of 200 km and my upper limit modern thickness of 250 km imply that the lithosphere has thickened at most $\sim$50 km in over the last $\sim$2.5 Gyr. I do not attempt to define a lower limit for the increase in lithosphere thickness.

[46] This lithospheric thickness is not much greater than that of younger continental platforms as indicated by seismology and the subsidence histories of platform basins [e.g., *Kaminski and Jaupart*, 2000]. The modern platform lithospheric thickness is at least 170 km, comparable to that of Archean lithosphere.

3.2. Physical and Mathematical Model

[47] I first identify secondary convection driven by local density contrasts within the thermal boundary layer as the main mechanism that provides heat flow beneath cratons. Mantle plumes (Appendix B) and basal drag from plate motions (Appendix C) provide only small amounts of heat flow. I select boundary conditions and coordinates for my models of secondary convection so that plumes and heat flow from basal drag are ignored.

[48] I model cratons in partial isolation rather than attempting to model the whole Earth since 3 Ga. To do this, I present scaling models and two-dimensional numerical models in the plane perpendicular to plate motions. The numerical approach is justified to some extent because basal drag tends to organize convection into rolls [*Richter*, 1973]. *Solomatov and Moresi* [2000] discuss three-dimensional effects on the real Earth and conclude that their effect on the laterally averaged properties that I consider is small. Three-dimensional effects include drag-driven flow beneath lithospheric keels [*Shapiro et al.*, 1999b], flow driven by

lateral density contrasts at the edges of the cratons [*Fowler*, 1985; *Reese et al.*, 1998, 1999], and the disruption of rolls by changes in plate motion.

3.2.1. Differential Equations

[49] To obtain results, I need to solve coupled heat transfer and force balance equations within an incompressible fluid. I discuss my modeling methods in terms of formal initial value and boundary value problems.

[50] The heat flow equation and the continuity equation for the chemical component ϕ are

$$\frac{\partial T}{\partial t} + \mathbf{V} \cdot \nabla T = \kappa \nabla^2 T, \quad \frac{\partial \phi}{\partial t} + \mathbf{V} \cdot \nabla \phi = 0, \tag{10}$$

respectively, where T is potential temperature, t is time, $\mathbf{V}$ is velocity, and there are no heat sources nor chemical sources. The vertical component of the force balance equation in three dimensions is

$$\frac{\partial \tau_{xz}}{\partial x} + \frac{\partial \tau_{yz}}{\partial y} + \frac{\partial \tau_{zz}}{\partial z} - \frac{\partial P}{\partial z} + \Delta \rho g = 0, \tag{11}$$

where x is the horizontal coordinate in the plane of the convection cell and y are orizontal coordinate perpendicular to that plane in the direction of plate motions, P is the "scalar" pressure, $\Delta\rho$ is the excess density (from temperature and composition) relative to some reference, and the deviatoric stress tensor and the strain rate are related by equation (8).

3.2.2. Scaling Model Boundary Conditions

[51] My scaling models constrain the laterally averaged heat flow into the base of the lithosphere using techniques collectively called parameterized convection beneath a stagnant lid. I assume that the convective heat flow and the lithospheric thickness are in steady state as in equation (9). This makes the initial conditions irrelevant. The spatial boundary conditions are implicit as the method yields only lateral averages. The upper part of the lithosphere (the stagnant lid) is fixed and rigid, and the surface temperature is constant 0°C (Figure 2). The basal boundary condition for temperature is that the underlying adiabatic mantle cools at a rate of 50 K Gyr^{-1} to its present potential temperature of 1300°C [*Abbott et al.*, 1994; *Galer and Mezger*, 1998]. The mechanical basal boundary condition is that the underlying mantle moves at a given velocity relative to surface plate in a direction perpendicular to the convention cells.

3.2.3. Spatial Boundary Conditions for Numerical Models

[52] My two-dimensional numerical models are confined within a 600-km-wide and 400-km-deep box (Figure 2). I impose a combination of artificial and natural boundary conditions at the sides, top, and base of the box. The in-plane flow from convection and the antiplane flow from plate motions are only coupled by the stress invariant in equation (8). I represent the antiplane flow with the antiplane velocity V_y and the in-plane velocity with the curl of the stream function $\mathbf{V}_{in} = \nabla \times (\psi \mathbf{j})$, where $\mathbf{j}$ is the unit vector in the y direction.

[53] The antiplane boundary condition for temperature is that all conductive and convective heat flow is within the plane of the model ($\partial T/\partial y = 0$). One temperature boundary condition is required at each in boundary. The in-plane boundary conditions for temperature are no horizontal heat flow at the sides ($\partial T/\partial x = 0$), the natural condition of constant temperature (0°C) at the top, and constant temperature (the mantle adiabat which decreases by 50 K Gyr^{-1}) at the bottom.

[54] Two mechanical boundary conditions are required at each in-plane boundary. To represent the rigid upper lithosphere, I set the stream function to zero at two rows of grids at the top of the box (Appendix D). This precludes obtaining the dynamic topography at the free surface associated with localized convection but has no effect the deeper part of the model. (One can extract the laterally average topography assuming isostasy.) I impose no horizontal flow ($\psi = 0$) and no vertical shear traction ($\partial^2\psi/\partial x^2 = 0$) at the side boundaries. The basal boundary that the first and third derivatives of the stream function perpendicular to the boundary and the first derivative of viscosity are equal to zero. This "permeable" boundary condition allows fluid at the (slowly changing) mantle adiabat to enter the domain by flowing vertically and dense material to sink out of the domain. The effect of this boundary condition is that the boundary does no work on the rest of the model [*Sleep*, 1975; *Moore et al.*, 1999].

[55] One antiplane mechanical boundary condition is needed at each boundary. The boundary conditions for antiplane velocity are free slip on the sides ($\partial V_y/\partial x = 0$), constant zero velocity at the top, and constant imposed plate velocity at the bottom.

[56] The boundary conditions for chemical lithosphere are similar to those for temperature; there is again one condition at each boundary. There is no horizontal flow at the sides and chemical component $\phi = 0$ for the permeable boundary at the base. The upper boundary condition is no flow perpendicular to the boundary. The permeable basal boundary condition lets entrained chemical lithosphere escape into the much larger volume of the rest of the mantle as it would in nature. If a no-flow boundary condition were used instead, all the initial chemical lithosphere remains trapped in the box of the model. In that case, entrained chemical lithosphere is swept back to the surface in upwellings as in the models of *De Smet et al.* [2000].

3.2.4. Initial Value Conditions for Numerical Models

[57] My initial value conditions at 3200 Ma are fairly simple, as I am mainly interested in the quasi-steady behavior that follows later. Mathematically, I must specify the temperature and the chemical component at every point in the domain of the model. I assume that the initial temperature is horizontally stratified except for a small perturbation at 40-km depth to start convection. I impose a conductive lid (with a linear thermal gradient) over adiabatic mantle with a potential temperature of 1460°C. The lid is 40 km thick in the models with no chemical component in section 3.3 and 60 km thick in the models with a chemical component in section 3.4. The initial condition for the chemical component ϕ in section 3.4 is horizontally stratified. I assume that the chemical component is either 0 or 1 and that its flat base is at 192.5-km depth (the grid centered at 190-km depth).

3.2.5. Material Properties in Models

[58] Many material parameters are reasonably constrained for the Earth and do not vary much with temperature and pressure. I keep these parameters spatially invariant within

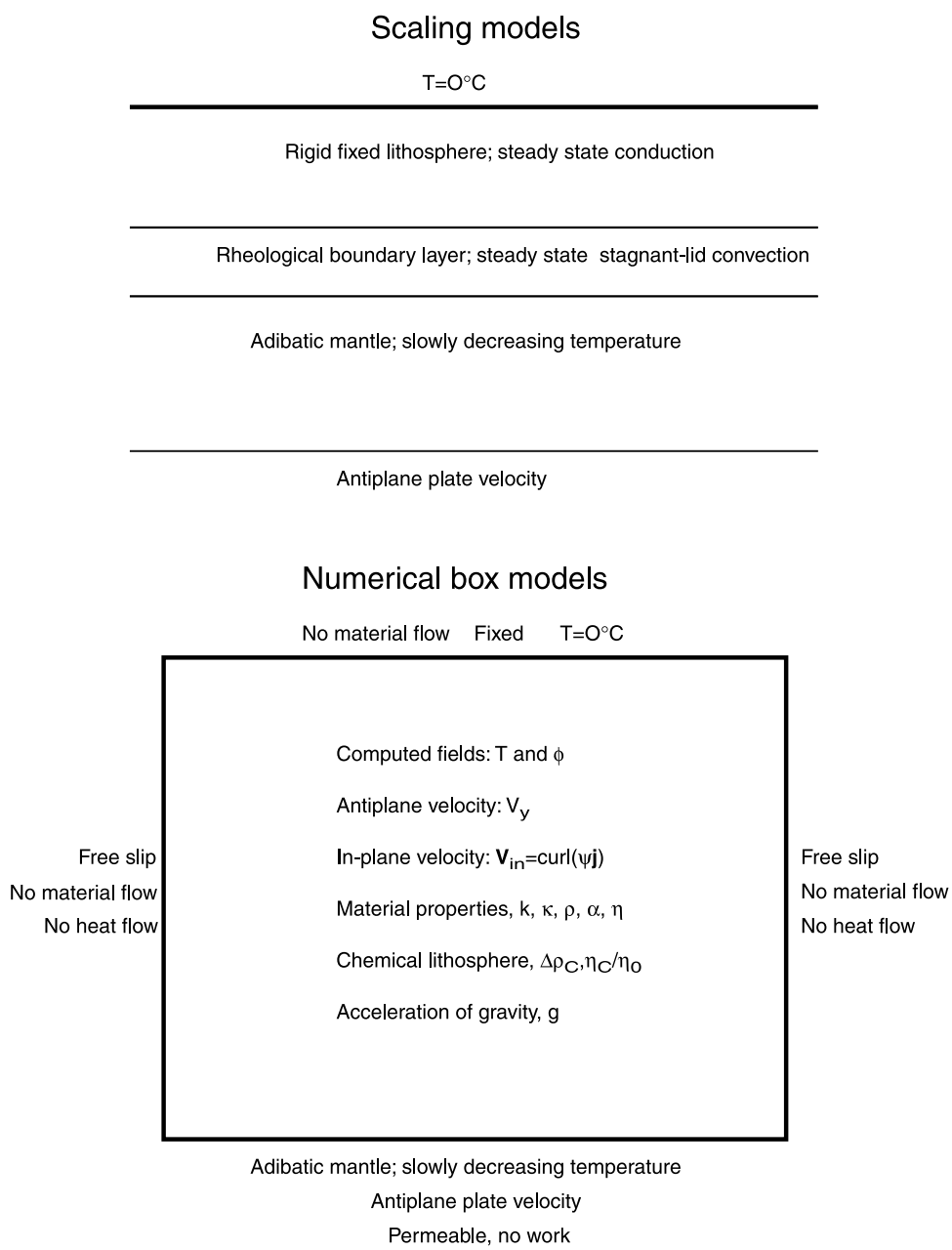

Figure 2. Mathematical boundary conditions for (top) my scaling models and (bottom) my two-dimensional numerical models. The scaling models give lateral averages and have no side boundary conditions. They are in quasi-steady state and have no starting conditions. The heat flow through the rheological boundary later determines the conductive thickness of the lithosphere. The mechanical basal boundary condition is that the deep mantle moves relative to the surface plate perpendicular to the plane of the figure and that the adiabatic temperature of the mantle changes slowly. Three mechanical conditions and one thermal condition are necessary on each boundary. The upper boundary is fixed (no perpendicular or parallel velocity) and at 0°C. The side boundaries have mirror symmetry so that there is free slip for in-plane and antiplane flow and no material or heat flow across the boundaries. The bottom boundary is permeable to let material in and out of the box. All entering material does so with no chemical lithospheric component and at the slowly changing mantle adiabat. The temperature and chemical component fields need to be given as initial conditions. The in-plane and antiplane velocities are obtained from them using a temperature-, pressure-, and composition-dependent nonlinear viscosity η, the density ρ, the thermal expansion coefficient α, the chemical density contrast $\Delta\rho_C$, and the acceleration of gravity g. I advect the temperature and chemical component fields with the in-plane velocity and conduct heat using the thermal conductivity k and the thermal diffusivity $\kappa \equiv k/\rho C$ to obtain new fields at the start of the next time step.

models and do not vary them between models. They include volume specific heat $\rho_C = 4 \times 10^6$ J m^{-3} K^{-1}, thermal diffusivity $\kappa = 0.75 \times 10^{-6}$ m^2 s^{-1}, thermal conductivity $k = 3$ W m^{-1} K^{-1}, thermal expansion coefficient $\alpha = 3 \times 10^{-5}$ K^{-1}, and the density $\rho = 3400$ kg m^{-3}. I keep the acceleration of gravity $g = 9.8$ m s^{-2} constant. I vary (the less well constrained) rheological parameters in equation (7) between models, that is, η_0, T_η, D_η, η_C/η_0, and n.

[59] The density contrast $\Delta\rho_C$ between cratonal lithosphere and normal mantle is reasonably constrained from petrology. *Doin et al.* [1997] use 60 kg m^{-3} in their numerical models and *Griffin et al.* [1999] find 50 kg m^{-3} from analysis of xenoliths and melting relationships. I use 50 kg m^{-3} in all the models that include this quantity in section 3.4. I assume that no chemical lithosphere exists in the models in section 3.3.

3.2.6. Approach to Modeling

[60] It is my intent to find reasonable combinations of the normal mantle rheological parameters η_0, T_η, D_η, and n and the viscosity ratio η_C/η_0 that satisfy the observations in section 3.1. The salient observation from xenoliths is that the cratonal lithosphere approached its modern thickness soon after it formed and has been more or less stable since then. It is conceivable that chemically buoyant material stabilizes cratonal lithosphere. I consider this hypothesis in section 3.4. Alternatively, buoyant chemical lithosphere may exist only above the rheologically active thermal boundary layer and play little part in the long-term stability of cratonal lithosphere. Data that bear directly on the existence of chemical lithosphere (magnetotellurics in section 2.2.2 and geoid in section 2.2.3) do not resolve this issue. I model the cases with and without buoyant cratonal lithosphere separately as different physical sets of parameters are important.

[61] The case without chemically buoyant lithosphere in section 3.3 involves complicated rheologies based on equations (7) and (8). A simple temperature-dependent rheology is not acceptable because it implies that the lithosphere should thicken with time from equation (9) as the convective heat flow waned as the mantle adiabat cooled [*Richter*, 1988].

[62] The main issue in the stability of a chemical lid in section 3.4 is that it does not get excessively entrained over time by the underlying convection. The chemical buoyancy and the viscosity contrast η_C/η_0 control the rate of entrainment. I keep the rheology simple so that I do not obscure this point. I consider only entrainment by convection beneath the boundary layer. *Lenardic et al.* [2000] consider the related issue of entrainment at subduction zones.

[63] My strategy is to use scaling to obtain simple relationships between material properties and observable quantities. This allows me to focus on parameter combinations compatible with observed constraints. I then present a successful two-dimensional numerical model for each simple case to appraise and illustrate the predicted behavior.

3.3. Stagnant Lid Convection Within an Isochemical Mantle

[64] In this section, I presume that chemically buoyant lithosphere does not act as a lid to convection and consider only density variations owing to temperature. That is, the parameters $\Delta\rho_C$ and η_C/η_0 and the variable ϕ are not involved in the calculations of this section.

[65] I partition my search for successful combinations of model parameters according to the stress from drag at the base of the plate. I find two models without chemical lithosphere that satisfy the observational constraints that the Archean craton lithosphere stabilized to about the modern lithospheric thickness and the temperature contrast across the rheological boundary layer is <300 K. First, in section 3.3.1, I presume that the stresses from drag are small enough that they do not affect the invariant in equation (8). This allows me to use traditional stagnant lid theory to obtain parameters for two-dimensional model L1. In section 3.3.2, I presume that the viscosity in equation (8) is nonlinear and plate drag is significant in the invariant. I modify existing stagnant lid results to model this possibility. In section 3.3.3, I examine which situation exists beneath cratons and present two-dimensional model N1.

3.3.1. Parameterized Convection With Weak Basal Drag

[66] In this section, stresses from basal drag do not significantly contribute to the invariant in equation (8) so that the plate velocity does not enter into the results. This allows me to apply well-known scaling results that relate heat flow to material properties.

[67] Numerical and laboratory studies relate the laterally averaged heat flow at quasi-steady state to material parameters at the base of the rheological boundary layer. I first present results that apply when the viscosity in equation (7) is not depth-dependent. The heat flow beneath a nearly rigid lid (the lithosphere) over an adiabatic half-space is

$$q_H = 0.47 k T_\eta \left[\frac{\rho g \alpha T_\eta}{\kappa \eta_H}\right]^{1/3}, \tag{12}$$

where η_H is the viscosity of the adiabatic half-space beneath the boundary layer [*Davaille and Jaupart*, 1993a, 1993b]. This boundary layer result is independent of the thickness of the adiabatic region beneath the boundary layer. The analogous expression for a nonlinear viscosity in equation (7) is more complicated

$$q_H = (a + bn) k T_\eta^{2(n+1)/(n+2)} (\alpha\rho g)^{n/(n+2)} (\kappa\eta_H)^{-1/(n+2)} \tau_{\mathrm{ref}}^{(n-1)/(n+2)}, \tag{13}$$

where a and b are dimensionless constants [*Solomatov and Moresi*, 2000].

[68] The quasi-steady lithospheric thickness in equation (9) is inversely proportional to the quasi-steady heat flow in equations (12) and (13). The relative change in lithospheric thickness with time results from the viscosity term in equation (13) and the temperature dependence of viscosity in equation (7). That is, ratio of the quasi-steady lithospheric thickness in the Archean over Z_R the present lithospheric thickness Z_P over in equation (9) is

$$\frac{Z_R}{Z_P} = \frac{T_R}{T_P} \exp\left[\frac{-\Delta T_R}{(n+2) T_\eta}\right], \tag{14}$$

where ΔT_R is the decrease of the mantle potential temperature since the Archean, T_R is mantle potential

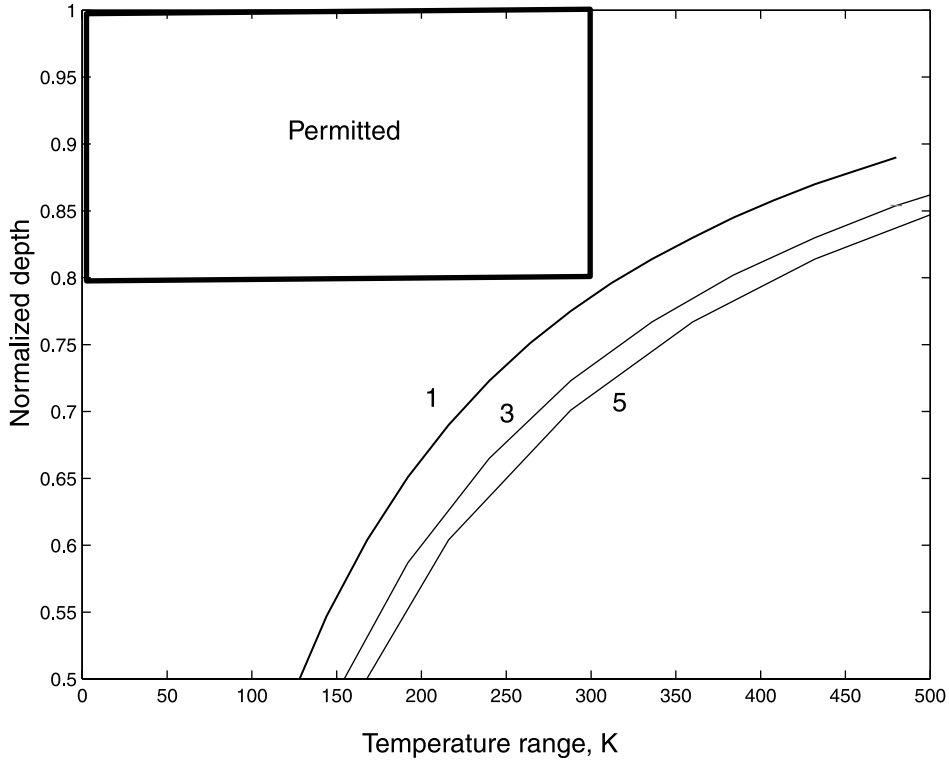

Figure 3. Lithospheric thickness at 2.5 Ga normalized to the modern thickness plotted as a function of the temperature range across the rheological boundary layer for linear ($n = 1$) and power law rheology ($n = 3$ and $n = 5$). All the curves miss the region permitted by xenolith studies. The temperature scale T_η increases clockwise on the curves.

temperature in the Archean, and T_P is the present mantle potential temperature.

[69] The second observable parameter is the temperature range across the modern rheologically active boundary layer. *Solomatov and Moresi* [2000] give the scaling relationship

$$\Delta T_{\text{rheo}} = 1.2(n+1)T_\eta. \tag{15}$$

That is, the thickness of the rheological active layer increases with increasingly nonlinear viscosity. A sufficiently large value of T_η precludes effectively rigid lithospheric mantle altogether. For example, *Lenardic* [1998] used a mildly temperature-dependent viscosity $T_\eta \sim 259$ K and his mantle lithosphere actively partook in the convection.

[70] Equations (12)–(15) do not include the effect of depth-dependent viscosity in equation (7). I include this by defining an effective temperature dependence of viscosity within the boundary layer. That is, if $D_\eta > 0$, the viscosity (as one moves upward within the thermal boundary layer) increases with decreasing temperature but decreases with decreasing depth. The temperature dependence obviously dominates because the upper part of the lithosphere is rigid. The pressure dependence makes the apparent change in viscosity with temperature in the boundary layer less than the intrinsic change from T_η in equation (7). I parameterize this effect by defining an apparent temperature dependence of viscosity within the rheologically active boundary layer,

$$T_A \equiv \left[\frac{1}{T_\eta} - \frac{2Z_H}{T_H D_\eta}\right]^{-1}, \tag{16}$$

where the factor of 2 arises since the thermal gradient is $\sim 1/2$ conductive gradient T_H/Z_H in the middle of the rheologically active boundary layer [*Sleep*, 1994]. I include depth-dependent viscosity in equations (12)–(15) by letting η_H be the viscosity at the base of the boundary layer and by replacing all T_η (outside the exponential) with T_A. I note that *Dumoulin et al.* [1999] considered the geothermal gradient at the top of the boundary layer T_H/Z_H to obtain equation (16) without the factor of 2.

[71] Equations (14) and (15) allow the predicted long-term relative change in lithospheric thickness and the predicted temperature range across the rheological boundary layer to be compared with observations. The relevant material parameters for depth-independent viscosity are the power law n and the temperature scale for viscosity T_η. The long-term cooling of the mantle in equation (14) and the present and past mantle potential temperatures are geological parameters. Depth-dependent viscosity in equation (16) involves the additional material parameter D_η.

[72] I represent the results of equations (14) and (15) by curves relating relative lithospheric thickening to the temperature range across the rheologically active boundary layer for various values of n (Figure 3). I let the modern lithosphere thickness be 250 km and let the modern potential temperature be 1300°C. I compare these conditions with those at 2500 Ma when the potential temperature was 1425°C. For purposes of illustration, I limit the permitted part of the observable parameter space to lithosphere thickening <50 km (20% relative to present thickness) as

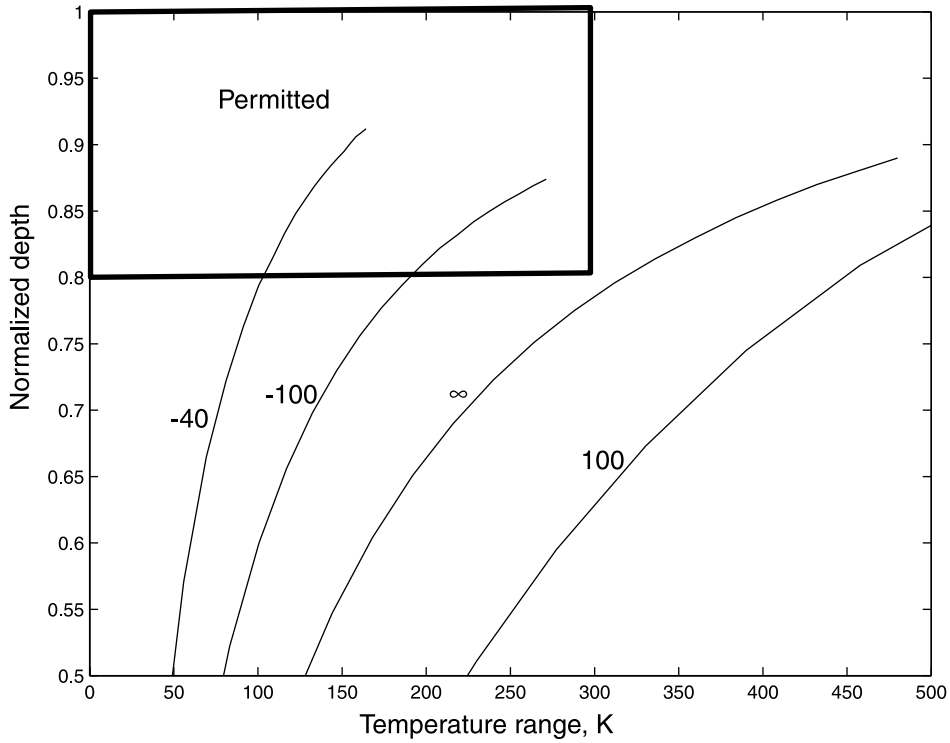

Figure 4. Lithospheric thickness at 2.5 Ga normalized to the modern thickness plotted as a function of the temperature range across the rheological boundary layer for values of the depth scale for viscosity D_η. The curves enter the permitted box for negative values of this parameter. The ∞ curve has no depth dependence and is the $n = 1$ curve from Figure 3.

the Earth's interior cooled 125 K. I limit the temperature range across the boundary layer to <300 K. None of the curves pass through the permitted box. This situation arises because using a large value of T_η to get a small relative change in lithospheric thickness in equation (14) implies an excessive temperature range in equation (15). Conversely, small T_η implies an excessive relative change in lithospheric thickness in equation (14). The nonlinear curves are further from the permitted region than the linear one.

[73] To illustrate the effects of depth-dependent viscosity, I plot curves of relative lithospheric temperature change versus the temperature contrast across the rheologically active layer for a linear rheology (Figure 4). The curves for positive D_η lie further from the permitted box than the curve without depth dependence. This results because positive D_η implies $T_A > T_\eta$ in equation (16), which increases the rheological temperature range in equation (15). The lithosphere also thickened more as the Earth's interior cooled over time. That is, the heat flow in equation (12) decreased from the direct effect of the viscosity η_H increasing as the Earth's interior cooled. This lower heat flow increased the lithospheric thickness in equation (9), which further increased η_H. The lithosphere thickens unstably as the mantle cools if the depth dependence is sufficiently strong [*Doin et al.*, 1997].

[74] Curves for negative D_η pass into the box (Figure 4). That is, $T_A < T_\eta$ in equation (16), which decreases the temperature range of the rheological boundary layer in equation (15). The temperature range becomes nearly independent of T_η as this parameter becomes large. That is, the viscosity then becomes mainly depth-dependent and not temperature-dependent.

[75] The case with negative D_η where the viscosity is significantly temperature-dependent is more likely to be relevant to the Earth. I illustrate the time dependence of lithospheric thickness by noting that the dominant parameter in the heat flow equation (14) is the viscosity at the base of the boundary layer η_H. To the first order, heat flow in equilibrium with the lithospheric thickness results if η_H at the base of the lithosphere stayed constant as the mantle cooled. That is, the increase in lithospheric thickness is crudely

$$\Delta Z_H \approx \frac{-D_\eta \Delta T}{T_\eta}. \tag{17}$$

For the example temperature change since the later Archean of 125 K and the 50-km upper limit for lithospheric thickness change, $-D_\eta$ is 17 and 40 km for T_η of 43 K (1 order of magnitude change over 100 K) and 100 K, respectively. This implies a viscosity decrease by factors of 360 and 12 over a 100 km increase in depth. It is clear that such viscosity gradients cannot extend to great depth, but it is conceivable that they could exist within limited regions like the seismic low-velocity zone [*Richards et al.*, 2002].

[76] I present a petrologically plausible two-dimensional numerical model (L1) (using initial conditions, boundary conditions, and parameters in section 3.2) to check that the scalings in equations (14), (16), and (17) give reasonable results and to illustrate the behavior of convection where

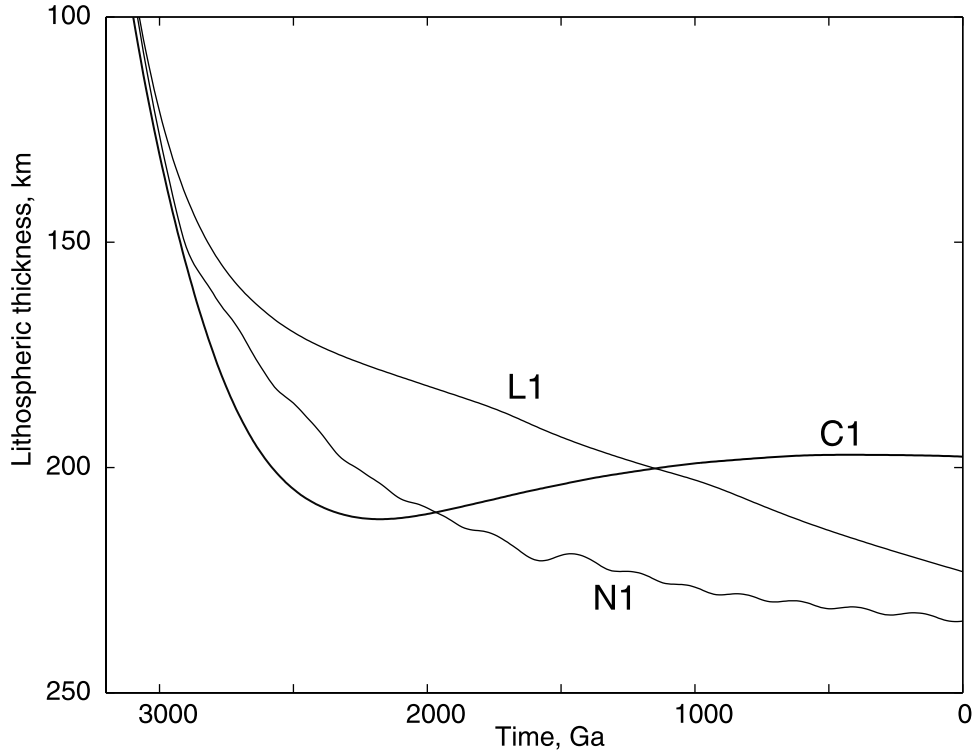

Figure 5. Lithospheric thickness as a function of time shown for models L1, N1, and C1.

viscosity decreases with depth. My viscosity structure represents the plausible effects of partial melt within the seismic low-velocity zone on rheology. For simplicity, I use round numbers. The viscosity along the present adiabat is constant at 10^{20} Pa s above 120 km depth; decreases 2 orders of magnitude between 120 and 220 km depth, increases 3 orders of magnitude between 220 and 320 km depth, and is constant at 10^{21} Pa s below that. This is a simple version of the viscosity model by *Forte and Perry* [2000] calibrated to get the base of the lithosphere at ~200 km. The intent of the viscosity increase is to impose a middle mantle viscosity compatible with glacial rebound data and to follow *Forte and Perry* [2000]. This region is beneath the boundary layer and has little effect on the heat flow. I assume a strong temperature dependence of viscosity with $T_\eta = 43$ K.

[77] The results are in agreement with the predictions of scaling. The lithospheric thickness defined by equation (9) increased from 182 to 223 km (45 km) after 2 Gyr compared with the expected increase from equation (17) of 50 km for $D_\eta = -22$ km (Figure 5). I plot the laterally averaged temperature, vertical conductive heat flow, and antiplane velocity in Figure 6. The laterally averaged heat flow at 2 Gyr is 23 mW m^{-2}. The viscosity at the base of the boundary layer is then 0.575×10^{19} Pa s at 182 km depth and using equations (12) and (16) yields a heat flow 19 mW m^{-2}, which is in tolerable agreement with predicted value. The predicted temperature range across the rheological boundary layer from equations (15) and (16) is 69 K. The computed temperature range is difficult to determine from the averaged heat flow in Figure 6 because model L1 is not exactly at steady state, so that the laterally averaged heat flow varies with depth within the rigid lithosphere. The

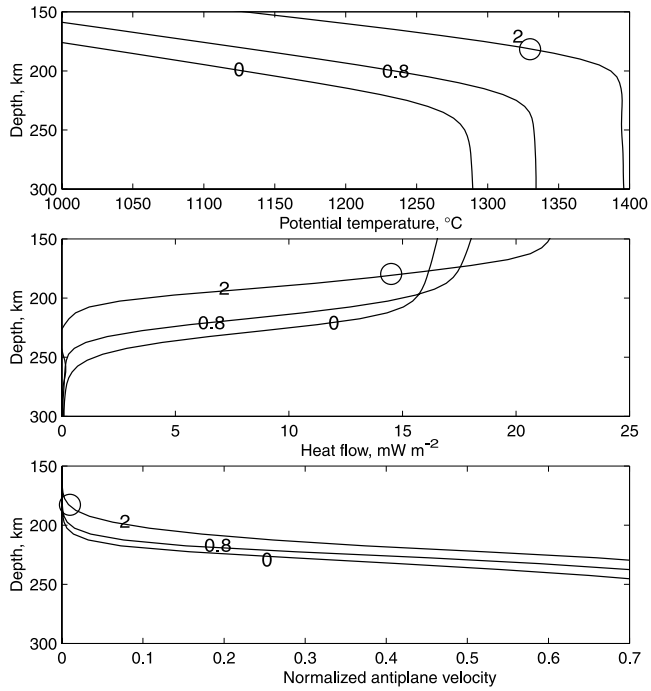

Figure 6. Laterally averaged properties for model L1. (top) Potential temperature, (middle) conductive heat flow, and (bottom) antiplane velocity normalized to plate velocity are shown for 0, 0.8, and 2 Ga. The circles denote the top of the rheologically active boundary layer at 2 Ga.

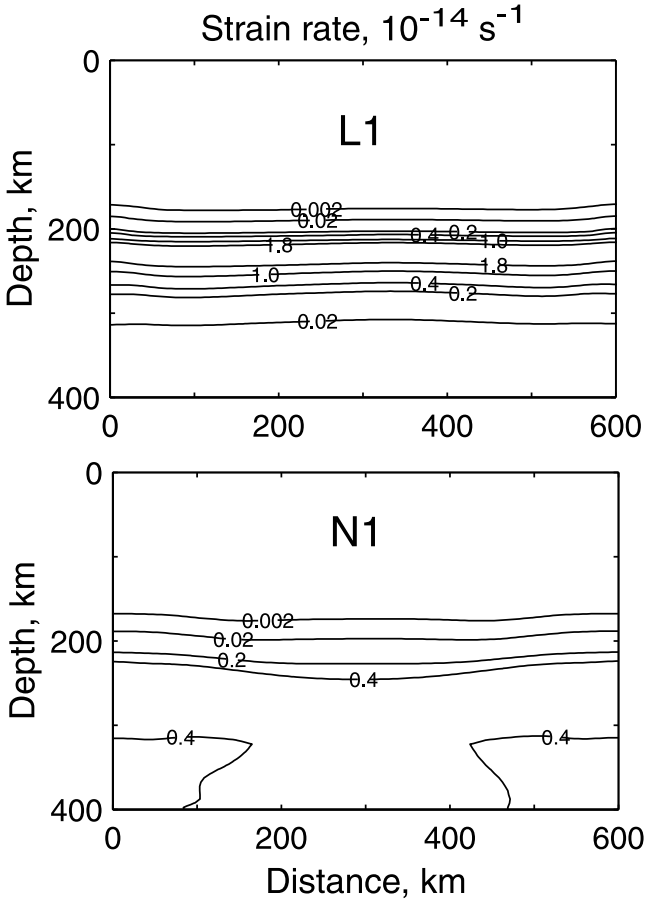

Figure 7. Present antiplane strain rate for models (top) L1 and (bottom) N1. The rapid strain rate is within a thin depth zone in L1 but a thick one in N1. Seismic anisotropy is a way of detecting this feature.

antiplane velocity in Figure 6 is a better measure of the depth to the base of rigid lithosphere. The computed temperature range ~70 K is in reasonable agreement with the model prediction.

[78] I present three additional lines of evidence at this time, which can be usefully appraised with two-dimensional numerical models. First, younger platform regions have lithosphere that is thinner than, but comparable to, cratonal lithosphere [e.g., *Kaminski and Jaupart*, 2000]. To appraise this effect, I started the model with thin lithosphere at 600 Ma, which yields an acceptable present lithospheric thickness of 195 km. Second, regions of high antiplane strain rate from plate motions are potentially detectable by seismic anisotropy (Figure 7). A thin zone of high strain rate occurs within the viscosity minimum just below the base of the lithosphere in the model. However, available shear wave splitting studies have not found this feature [*Silver et al.*, 1999].

[79] Third, petrological studies reviewed in section 2.1 indicate that lithospheric cratonal provinces have remained attached to their overlying crustal geological provinces since the cratons stabilized. The antiplane velocity in Figure 6 is a measure of how fixed material is to the overlying lithosphere. For a plate velocity of 10^{-9} m s^{-1}, the material with a normalized velocity of 0.001 moves 75 km in 2.5 Gyr. The actual movement is somewhat less as the direction of the plate movement changes as plate tectonics reorganizes. Mathematically, the expected displacement is 75 km divided by square root of the number of plate reorganizations since 2.5 Ga. For example, nine reorganizations imply 25 km of movement. That is, lithospheric material stays with its overlying crust if the normalized antiplane velocity in Figure 6 is less than a factor of a few times 0.001.

3.3.2. Parameterized Convection With Strong Basal Drag

[80] The stress invariant in equation (8) couples flow from basal drag with flow within two-dimensional rolls for a nonlinear rheology. It is not a priori evident whether the contributions of basal drag or those of the localized convection dominate the stress invariant beneath cratons. In section 3.3.1, I assumed that the effect of basal drag on the invariant is minor and applied well-known scaling relationships for nonlinear flow. A second relatively simple case arises when the basal drag stress is much greater than the stresses from convection. I examine this case to obtain scaling relationships for the observable properties of the laterally averaged heat flow and the temperature range across the rheological boundary layer. In section 3.3.3, I then examine the conditions whereby this situation can originate beneath cratons and conclude that that they are marginally plausible. I present a two-dimensional numerical model N1 to illustrate some properties of this case.

[81] In the case of large basal drag and aligned convective rolls, the strain rate associated with localized convection ε'_{ij} in equation (8) is related to the stress tensor τ_{ij} associated with localized convection by

$$\varepsilon'_{ij} = \frac{\tau_{ij}}{2\eta}\left[\frac{\tau_D}{\tau_{\mathrm{ref}}}\right]^{n-1}, \tag{18}$$

where τ_D is the stress from plate drag. The viscosity for localized convection then behaves as if it were linear. The "pseudolinear" apparent viscosity for localized convection is then

$$\eta_{\mathrm{app}} = \eta\left[\frac{\tau_{\mathrm{ref}}}{\tau_D}\right]^{n-1}, \tag{19}$$

which implies that high basal shear traction reduces the apparent viscosity for localized convection. The scaling relationships for linear convection then give heat flow in equation (12) and the temperature range across the basal boundary layer in equation (15).

[82] The time-dependent behavior of heat flow from equations (19) and (12) involves an intrinsic change of the viscosity η in equation (7) as the Earth cooled, the effect of this change on the basal drag, and the effect of plate velocity on basal drag. I obtain dimensional results by representing simple shear within the region beneath the lithosphere as an equivalent channel with a constant viscosity. Without loss of generality, I define the reference plate velocity to be

$$V_{\mathrm{ref}} \equiv \frac{\tau_{\mathrm{ref}}\Delta Z_{\mathrm{ref}}}{\eta_{\mathrm{ref}}}, \tag{20a}$$

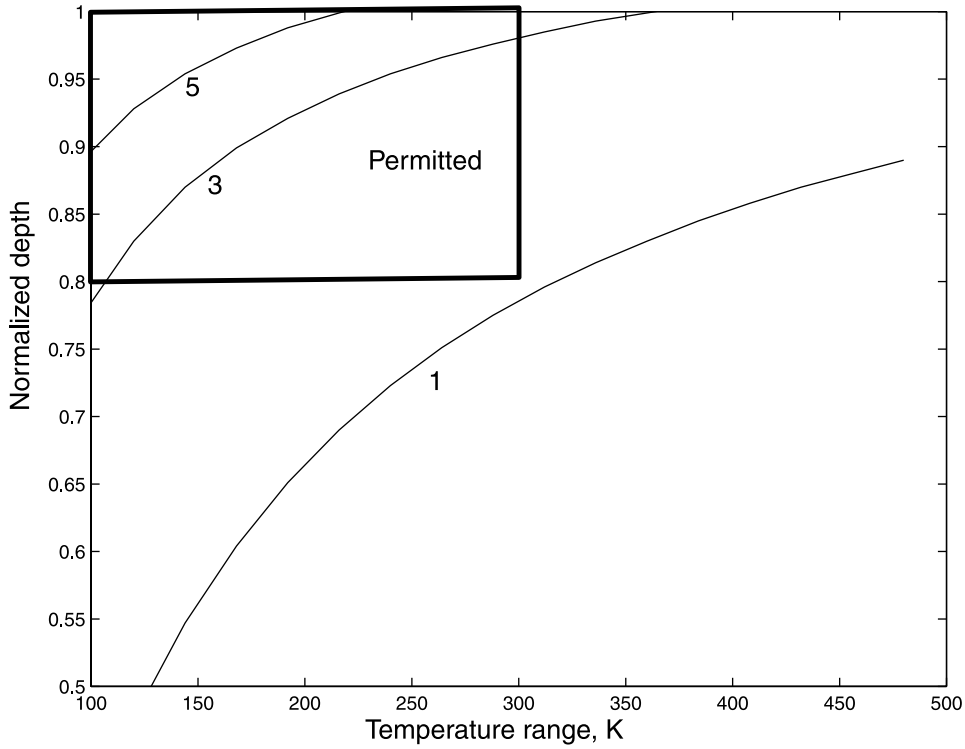

Figure 8. Lithospheric thickness at 2.5 Ga normalized to the modern thickness is plotted as a function of the temperature range across the rheological boundary layer for pseudolinear rheology. The linear curve from Figure 3 is unchanged. The nonlinear curves are mostly within the permitted box.

where ΔZ_{ref} is the reference channel thickness and η_{ref} is a reference viscosity. The plate velocity, in general, is

$$V_{\text{plate}} \equiv \frac{\tau_D^n \Delta Z}{\tau_{\text{ref}}^{n-1} \eta}, \tag{20b}$$

where the viscosity is η at the reference shear traction and the channel has thickness ΔZ. The apparent viscosity in equation (19) is then

$$\eta_{\text{lapp}} = \eta_{\text{ref}}^{(n-1)/n} \eta^{1/n} \left[\frac{\Delta Z V_{\text{ref}}}{\Delta Z_{\text{ref}} V_{\text{plate}}}\right]^{(n-1)/n}, \tag{21}$$

which implies that the heat flow in equation (12) is proportional to

$$q_H \propto \eta^{-1/3n} \left[\frac{\Delta Z}{V_{\text{plate}}}\right]^{(n-1)/3n} \propto \exp\left[\frac{-\Delta T}{3nT_\eta}\right], \tag{22}$$

where the second proportionality represents only the temperature dependence of viscosity in equation (7).

[83] The inverse dependence of heat flow and hence lithospheric thickness on plate velocity is difficult to test as the average plate velocity over the thermal timescale of the lithosphere, the last few hundred million years, is unknown. A complicating phenomenological issue is that cratons with thin lithosphere might move faster because they apply less total drag to their plates.

[84] At the pseudolinear limit in equation (22), the effective temperature dependence of apparent viscosity as the Earth cooled scales with nT_η, while the temperature range across the regionally active boundary layer is that for a linear fluid in equation (15). Curves relating these parameters are within the permitted region (Figure 8). I therefore continue to discuss this initially promising case.

3.3.3. When Is Basal Drag Important?

[85] To this point, I have examined two end-member cases of nonlinear convection. In section 3.3.1, I considered well-known parameterizations where the basal shear traction does not significantly affect the invariant in equation (8). In section 3.3.2, I considered the case where basal shear traction dominates the invariant. The relative magnitudes of the two contributions to the invariant determine whether one of the special cases applies or whether the basal shear traction and convective stresses are comparable.

[86] The mathematics are simplified when drag aligns localized convection into rolls because the drag terms and the convection terms are not multiplied by each other in the invariant. That is, the stress invariant is

$$\tau = \left[\tau_D^2 + \tau_V^2\right]^{1/2}, \tag{23}$$

where τ_V is the stress invariant for convection normalized so that it would give the shear traction in simple shear. I obtain the relative magnitudes of the two terms in the invariant in equation (23) by considering thermodynamic work done by localized convection. The viscous dissipation per surface area in a convecting fluid is proportional to the heat transferred through the fluid by localized convection

$$q_W = \left[\frac{\alpha g \Delta Z}{C}\right] q_V, \tag{24}$$

where q_V is the heat flow by localized convection, C is the specific heat per mass at constant pressure, and ΔZ in equation (20b) is in general the thickness of the convecting region [e.g., *Stacey*, 1977, equations (3) and (14)]. Dividing by the convecting layer thickness, the average dissipation per volume is dimensionally

$$\frac{\tau_V^2}{\eta} = \frac{\alpha g q_V}{C}, \tag{25}$$

where η is the apparent viscosity in the volume of interest. The invariant from basal drag is

$$\frac{\tau_D^2}{\eta} = \frac{\eta V_{\text{plate}}^2}{\Delta Z^2}. \tag{26}$$

The ratio of the two contributions to the invariant is

$$\frac{\tau_V^2}{\tau_D^2} = \frac{\alpha g q_V \Delta Z^2}{C \eta V_{\text{plate}}^2}. \tag{27a}$$

All the parameters on the right-hand side of equation (27a) are constrained except for the layer thickness and the apparent viscosity. For $\alpha = 3 \times 10^{-5}$ K^{-1}, $q = 20$ mW m^{-2}, $\rho C = 4 \times 10^6$ J m^{-3} K^{-1}, $\rho = 3400$ kg m^{-3}, and $V_{\text{plate}} = 10^{-9}$ m s^{-1} ($\sim$30 mm yr^{-1}), equation (27a) becomes

$$\frac{\tau_V}{\tau_D} = 0.71 \quad Z_{100} \eta_{20}^{-1/2}, \tag{27b}$$

where the thickness Z_{100} of the basal shear layer is in units of 100 km and the viscosity η_{20} is in units of 10^{20} Pa s.

[87] The upper limit on basal shear traction of a few megapascals in section 2.3.1 constrains the layer thickness and its viscosity in equation (27b). That is, the basal traction in these units is η_{20}/Z_{100} MPa. This implies that the stresses from basal drag and convection are comparable for viscosity in the expected range. Conversely, it is unlikely that the ratio of the stresses in equation (27b) is so low that the pseudolinear limit in equation (22) applies. The equivalent layer thickness is unlikely to be less than a few tens of kilometers. The basal traction then constrains the viscosity to be less than $\sim 10^{20}$ Pa s.

[88] I constrain the transition from pseudolinear behavior to nonlinear behavior by using the parameterized heat flow equation (12) to dimensionally eliminate viscosity from equation (25),

$$\tau_V = \frac{\rho \alpha g k T_\eta^2}{q_V}, \tag{28}$$

Similarly, eliminating the viscosity from equation (27a), the ratio of the two contributions to the invariant is

$$\Pi_\tau \equiv \frac{\tau_V}{\tau_D} \approx \frac{\Delta Z q_V^2}{V_{\text{plate}}^2 \rho C k T_\eta^2}, \tag{29}$$

where the heat flow is that predicted by the pseudolinear limit using equation (12).

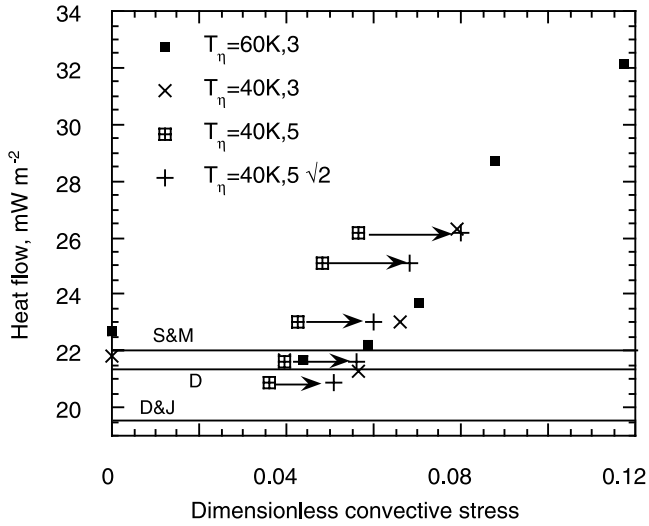

Figure 9. Laterally averaged heat flow through the boundary layer plotted as a function dimensionless convective stress as given by Π_τ in equation (46). If the pseudolinear assumption holds, the heat flow is predicted to be in the region defined by straight lines for linear scaling results of (D&J) *Davaille and Jaupart* [1993a, 1993b], (D) *Dumoulin et al.* [1999], and (S&M) *Solomatov and Moresi* [2000]. Models assuming $n = 3$ and $T_\eta = 60$ K (solid squares), $n = 3$ and $T_\eta = 40$ K (crosses) define the same trend, which intersects the pseudolinear region at $\Pi_\tau = 0.06$. The trend for $n = 5$ and $T_\eta = 40$ K (crossed squares) intersects the pseudolinear region at $\sim$0.04. The $n = 5$ points (pluses) fall within the $n = 3$ trend when multiplied by $\sqrt{2}$ as expected from the scaling. Fully linear calculations are shown at the limit of zero convective stress.

[89] To continue, the apparent viscosity in equation (8) depends on the invariant to the $n - 1$ power. That is,

$$\eta_{\text{app}}^{-1} \propto \left[\tau_D^2 + \tau_V^2\right]^{-(n-1)/2} \propto \tau_D^{n-1}\left[1 - \frac{(n-1)\tau_V^2}{2\tau_D^2}\right] \propto \tau_D^{-(n-1)}\left[1 - \frac{(n-1)\Pi_\tau^2}{2}\right], \tag{30}$$

where the second proportionality uses the first terms of the Taylor series and the third uses the dimensionless parameter in equation (29) expressed in terms of physical parameters.

[90] I compute temporally and laterally averaged heat flow from a series of number models by varying Π_τ in equation (29) to appraise the proportionality in equation (30). For convenience, I use the box for the linear model L1 parameters in section 3.3.1 with the modifications that the basal temperature is constant so that steady state may be approached and that viscosity is not depth-dependent. I vary the power n and the temperature dependence T_η, I adjust the other parameters so that the expected pseudolinear heat flow is the same for all the models. The models confirm that the heat flow depends of n and Π_η, but not explicitly on T_η (Figure 9). The pseudolinear prediction breaks down for $\Pi_\tau \approx 0.06$ and 0.04, respectively, for $n = 3$ and 5. I illustrate the expected dependence of apparent viscosity and hence heat flow on $\sqrt{(n-1)/2}$ by moving the $n = 5$ points over by a factor of $\sqrt{2}$ into the array of $n = 3$ points.

[91] From equation (27b), it is unlikely that the dimensionless ratio Π_τ is that low as low as 0.06 beneath cratons. It is plausible that the ratio is low enough that some of the inferences about pseudolinear behavior are qualitatively correct.

[92] I compute a nonlinear model N1 to illustrate some of the properties of parameter range where basal drag is significant but does not overwhelm the invariant in equation (8). I use the boundary conditions and parameters from the linear model L1 given in section 3.2 with the following modifications. The plate velocity is 10^{-9} m s^{-1} ($\sim$30 mm yr^{-1}). The depth dependence of viscosity at a given temperature increases the basal drag stress as the lithosphere approaches its present depth. Viscosity along an adiabat is constant between the surface and 220 km depth, increases a factor of 31.8 between 220 and 320 km depth, and is constant below that. The viscosity coefficient η_0 is 0.12×10^{21} Pa in equation (7) at the present mantle potential temperature of 1300°C. The reference shear traction and the traction at the base of oceanic lithosphere at the plate velocity of 10^{-9} m s^{-1} is 0.56 MPa. From equation (20b), the drag on oceanic crust moving at 3 times this rate is a factor of $\sqrt[5]{3}$ greater or 0.70 MPa, which is a factor of $\sim$2 greater than the acceptable range section 2.3.1. The temperature scale is 43 K as in the linear model L1. As in the linear model, I start thin lithosphere at 3.2 Ga and let the Earth's interior cool by 50 K Gyr^{-1}.

[93] The model shows the expected feature of pseudolinear convection that the lithosphere defined by equation (9) thickens slowly after 2.5 Ga (Figure 5). Quantitatively, the lithosphere thickness in Figure 5 increased by a factor of 1.165 between 2 and 0 Ga. Over this time, the model viscosity (at the reference stress along the mantle adiabat) increased by a factor of 10. Equation (22) predicts that the heat flow decreased by a factor of $10^{1/15} = 1.166$, which is in reasonable agreement with the model results. The laterally averaged antiplane shear traction increased from 0.495 to 0.877 MPa, a factor of 1.77, over this model time. The predicted increase from viscosity alone in equation (20b) is a factor $10^{1/5} = 1.58$. The modest difference occurs because viscosity increases with depth below 220 km in the model. The computed value of the modern shear traction is acceptable with regard to the force balance within plates in section 2.5.1.

[94] The present computed lithosphere thickness of a model started with thin lithosphere (197 km) at 600 Ma, which is acceptable for modern platform lithosphere. A thick zone of moderate strain rates extends toward the base of the model (Figure 7).

[95] However, the temperature range across the rheologically active boundary layer is $\sim$200 km is >103 km expected for pseudolinear convection ($n = 1$ in equation (15)) (Figure 10). This thickness is less than the 310 km expected from equation (15) for nonlinear convection ($n = 5$ in equation (15)). This discrepancy occurs because the convection in the model is very time-dependent, like convection (without basal drag) cooled from above in a fluid with a nonlinear viscosity [*Solomatov*, 1995; *Reese et al.*, 1998, 1999; *Kawada and Honda*, 1999; *Solomatov and Moresi*, 1997, 2000]. That is, the thermal boundary layer is stagnant at most times. Once a downwelling starts, stress concentrations form in the region of the downwelling, and the apparent viscosity decreases. The downwelling grows, producing still higher stresses, and much of the boundary layer delaminates in an avalanche. The boundary layer then slowly thickens until the next avalanche occurs. This episodicity of heat flow to the base of the lithosphere causes the lithospheric thickness in Figure 5 to be nonmonotonic.

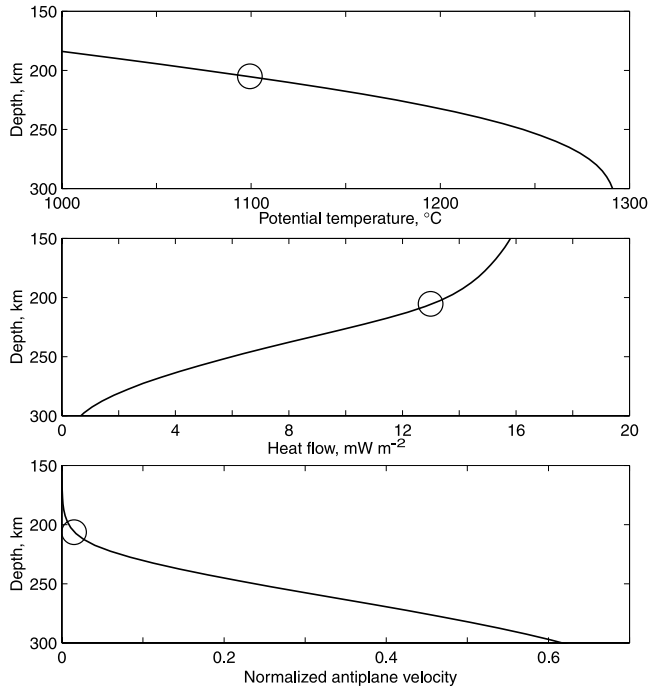

Figure 10. Laterally averaged properties for model N1. (top) Potential temperature, (middle) conductive heat flow, and (bottom) antiplane velocity normalized to plate velocity are shown for the present. The circles denote the top of the rheologically active boundary layer.

[96] I illustrate periods of relative quiescence and an episodic avalanche with the computed temperature field at 2, 0.8, 0 Ga in Figure 11. Downwellings occur at only the corners at 2 and 0 Ga. These downwellings remain fixed because the symmetry boundary condition on the sides of the numerical box removes degrees of freedom. Still, the vigor of these downwellings is time-dependent. An avalanche is underway in the middle of the model at 0.8 Ga.

[97] I quantify the nonlinear behavior by plotting the ratio $\tau_D^2/(\tau_D^2 + \tau_{\dot{V}}^2)$ as a function of position in Figure 12. This quantity is 1 when antiplane strain rate dominates the invariant and the pseudolinear approximation is appropriate. The values of the parameter near the top of the active boundary at 200 km depth are relevant to how far convection penetrates upward into lithosphere. The parameter over much of the model approaches 1 at 0 Ga except near the sides where downwelling occurs. The parameter has values $\sim$1/2 indicating that the effects of convection and basal drag on the invariant are comparable near and above the avalanche at 0.8 Ga.

[98] Qualitatively, the lateral and temporal averages of dissipation used to derive equations (29) and (30) give an over optimistic assessment of when the pseudolinear limit applies or equivalently pseudolinear behavior breaks down for Π_τ much less than 1 (Figure 9). The dissipation

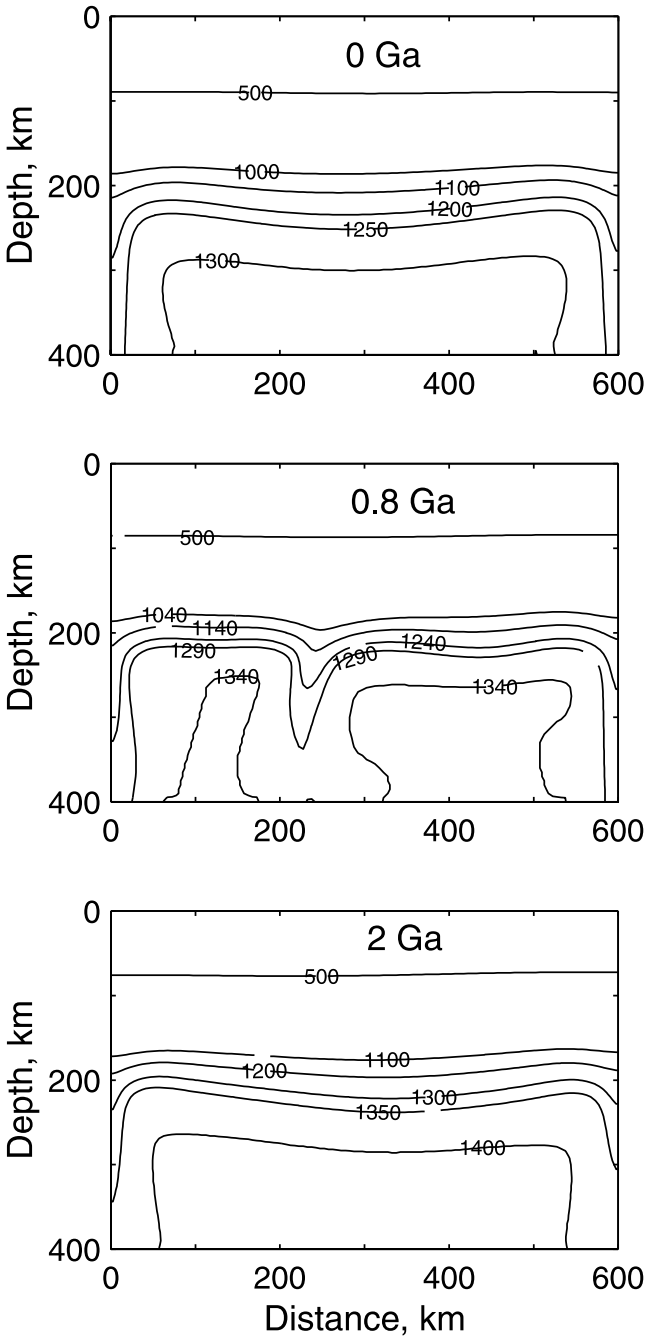

Figure 11. Potential temperature of model N1 at 0, 0.8, and 2 Ga. An avalanche is underway at 0.8 Ga in the center of the middle panel. Stress concentrations occur in and around the avalanche.

associated with convection concentrates in the vicinity of the downwellings at the time of avalanches. The dissipation associated with basal drag covers the broad base of the lithosphere at all times. The behavior around the downwellings controls the time-averaged thickness of the boundary layer. Heat flow relates to the frequency of avalanches and hence the pseudolinear flow early in their evolution. Real avalanches are three-dimensional events where drag and convection are not orthogonal as assumed in deriving equation (29).

[99] The large thickness of the rheological boundary layer is a serious drawback to pseudolinear models. The large basal tractions required for this behavior are a second drawback. There is also little evidence that the base of the lithosphere episodically fails in large avalanches though admittedly there has been little effort to recognize this effect. Pseudolinear convection is at the margin of reasonability, like the linear model L1 with a strong viscosity decrease with depth. Conversely, moderate basal tractions affect the stress invariant. Global nonlinear models of convection beneath cratons need to include moving cratons and hence basal drag in some way.

3.4. Chemically Buoyant Lithosphere

[100] The chemical buoyancy is a prime suspect for the longevity of cratonal lithosphere [*Jordan*, 1981; *Richter*, 1988; *Doin et al.*, 1997; *Shapiro et al.*, 1999a]. In that case, the base of chemically buoyant lithosphere defines a lid to localized convection within the mantle below. I extend the scaling relationships in section 3.3 and introduce additional

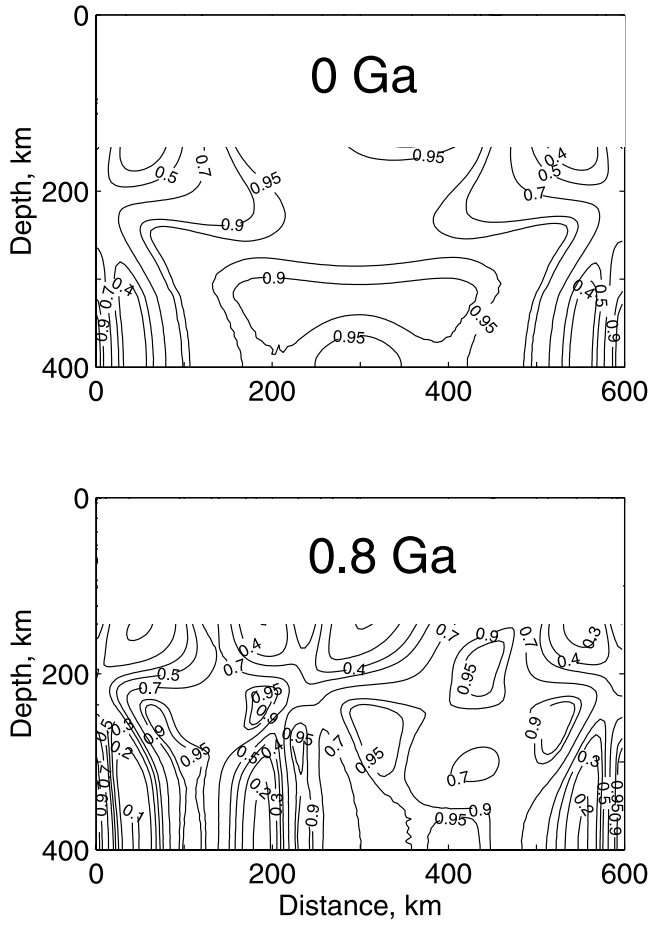

Figure 12. Dimensionless ratio $\tau_D^2/(\tau_D^2 + \tau_V^2)$ contoured for model N1 at 0 and 0.8 Ga. The contribution of convection to the stress invariant is significant near the edges at 0 Ga. The contributions of convection and antiplane strain are comparable at 0.8 Ga when an avalanche is in progress. The rigid lithosphere is whited out to focus attention on this invariant in the fluid region where deformation occurs.

scaling relationships to investigate this problem. As in section 3.3, I investigate quasi-steady behavior associated with the persistence of cratonal lithosphere, rather than how it formed in the first place. I describe the properties of the chemical layer with two simple parameters: the chemical density deficit with normal mantle $\Delta\rho_C$ and the ratio of the viscosity of the two layers η_C/η_0 in equation (7).

[101] I reduce the number of model parameters in my dimensional relationships by two by making the rheology linear and independent of depth. The effect of nonlinear rheology is unclear as the boundary layer and the immediately overlying chemical layer fail as avalanches. Three-dimensional models are required. The effect of depth-dependent viscosity is expected to be minor as the depth range in the boundary layers at the interface at the base of the chemical layer is not particularly great. To first order, depth dependence is accounted for by using T_A in equation (16) rather than T_η in scaling relationships that involve the temperature range across the boundary layer.

[102] I concentrate on when the chemical layer loses its identity by entraining normal mantle from below and when the layer itself is entrained into the normal mantle. My objective is to find conditions where the cratonal lithosphere persists as is inferred from xenoliths in section 2.1. I again partition models, this time with respect to the viscosity contrast η_C/η_0. In section 3.4.1, I begin by assuming that chemically buoyant lithosphere exists above normal mantle to obtain scaling relationships for entrainment where $\eta_C/\eta_0 = 1$, which imply that the chemical layer gets entrained. In Appendix E, I consider conditions where the chemical layer convects internally rather than acting as a rigid lid. This situation results in rapid entrainment of the chemical layer. I obtain an expression for the temperature contrast across the normal mantle boundary layer beneath the chemical lithosphere in the process. In section 3.4.2, I consider when η_C/η_0 becomes great enough to prevent entrainment of the chemical layer. I appraise and illustrate the scaling inferences with two-dimensional numerical model C1 in section 3.4.3.

[103] I do not consider processes that might renew chemical lithosphere, such as the formation of depleted residuum from the partial melting of plume material and the formation of cumulates from the partial crystallization of the melts so generated. I also do not explicitly consider the changes of the rheology of the chemical lithosphere over time from metasomatism. Both these processes occur to some extent, but I do not have a good way to quantify their importance. Modeling them would require several more poorly constrained petrologic and rheological parameters and would require explicit modeling of plumes and partial melting and hence a lot of petrologic insight. I acknowledge their possible importance but concentrate on the simpler situation where the chemical lithosphere formed in the Archean.

3.4.1. Gradual Entrainment of Buoyant Cratonal Lithosphere

[104] A chemically buoyant lid over localized convection actively participates in the flow. I qualitatively illustrate this by considering a region around a downwelling (Figure 13). The underlying flow entrains the chemical layer and draws it into a cusp. The buoyancy of the chemical material in the cusps resists further downwelling. Mathematically, from equation (11), the lateral density contrast in the cusp produces a body force. The downwelling entrains a wisp of material at the tip of the cusp and carries it deep into the lower fluid, that is, the rest of the mantle.

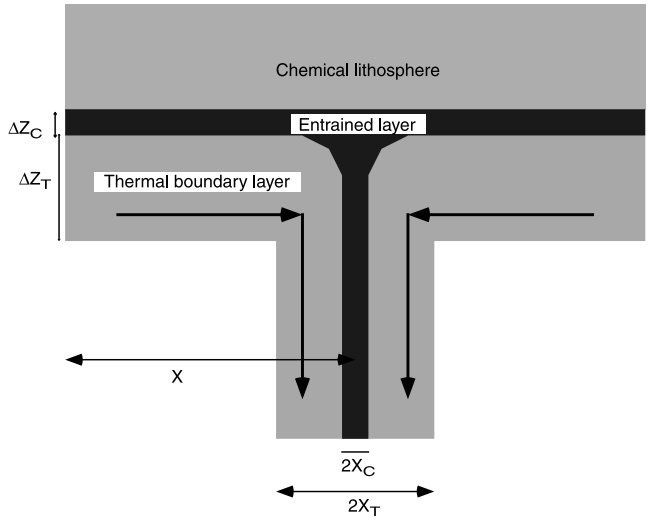

Figure 13. Entrainment of material into a schematic downwelling. I use the force balance in the downwelling to constrain the ratio X_C/X_T for entrainment limited by the buoyancy of the chemical layer. I use simple shear to constrain the horizontal flux within the entrained chemical layer of thickness ΔZ_C. The heat flux within the thermal boundary layer is proportional to its thickness ΔZ_T. These relationships allow entrainment rate to be related to heat flow.

[105] My objective is to determine the volume flux of material into the wisp and not the detailed fate of the wisp once it is mixed into the normal mantle. To do this, I dimensionally solve equation (11). For simplicity, I assume linear rheology. I consider a region within the craton where the base of the chemical layer is more or less flat. That is, I ignore the complications of entrainment in a much larger flow pattern [*Doin et al.*, 1997], flow at cratonal edges [*Shapiro et al.*, 1999b], and subduction zones [*Lenardic et al.*, 1993, 2000, 2003].

[106] The temperature contrasts associated with localized convection are small enough that entrainment rather than wholesale overturn is the relevant process. To show this, I note from equation (15) that the scaling for density contrasts within the rheologically active boundary layer is dimensionally

$$\Delta\rho_T = \rho\alpha T_\eta. \tag{31}$$

For example, $T_\eta = 43$ K implies $\Delta\rho_T = 4$ kg m^{-3}. The probable chemical density contrast is much larger, $\sim$50 kg m^{-3}.

[107] I obtain the rate of gradual entrainment resisted by buoyancy following *Sleep* [1988], by considering the balance of forces in a downwelling (Figure 13). This formalism is well known. *Lenardic et al.* [1993] used it for the similar problem of entrainment of continental crust into the mantle of Venus. *Davaille et al.* [2002] extend it to the case of two convecting fluids with different nontemperature-dependent viscosities and compare it with laboratory experiments. I consider the interface between two fluids with temperature-

dependent viscosity and two-dimensional convective rolls. My dimensional results are the two-dimensional analogs of the cylindrical plumes considered by *Davaille et al.* [2002]. I formulate my results in terms of heat flow, a well-constrained parameter for stable cratons.

[108] I begin by presuming that the boundary layer limit applies where the width X of the cell is much greater than the width X_T of the thermal downwelling and that width of the chemical downwelling X_C is small compared to the width of the thermal downwelling. The vertical shear traction from viscosity balances the buoyancy forces balance on the downwelling material:

$$\frac{\eta V}{X} \approx g[\Delta\rho_T X_T - \Delta\rho_C X_C], \tag{32}$$

where η is the viscosity of the mantle surrounding the downwelling and V is the velocity of the downwelling, The dimensional rate at which entrained material is dragged down is

$$X_C V = \frac{g X X_C}{\eta}[\Delta\rho_T X_T - \Delta\rho_C X_C]. \tag{33}$$

This rate is at a maximum when

$$X_C = \frac{\Delta\rho_T X_T}{2\Delta\rho_C}. \tag{34}$$

The maximum is a dimensional scaling because the chemical rate in equation (33) is a weak function of X_C.

[109] The rate $-\partial Z_C/\partial t$ at which the chemical layer thins is relevant to whether the layer persists over geological time. I relate this quantity to the observed quantity heat flow using the rate $\partial Z_T/\partial t$ at which convection thins the thermal boundary layer. Mass balance implies that the ratio that

$$\frac{X_C}{X_T} = \frac{-\dfrac{\partial Z_C}{\partial t}}{\dfrac{\partial Z_T}{\partial t}}. \tag{35}$$

The rate at which this chemical layer thins is from equations (34) and (35)

$$-\frac{\partial Z_C}{\partial t} = \frac{\partial Z_T}{\partial t}\left[\frac{\Delta\rho_T}{2\Delta\rho_C}\right]. \tag{36}$$

The laterally averaged convective heat flow using equation (31) for the temperature contrast is dimensionally

$$q = \rho C T_\eta \frac{\partial Z_T}{\partial t}. \tag{37}$$

Combining equations (31), (36), and (37) yields the relationship between heat flow and the entrainment rate

$$-\frac{\partial Z_C}{\partial t} = q\left[\frac{\rho\alpha}{2\rho C\Delta\rho_C}\right], \tag{38}$$

which is independent of the viscous temperature scale T_η and depends inversely on the chemical density contrast.

[110] The entrainment rate predicted by equation (38) would preclude long-lived chemical cratons. As an example, I use parameters from the models of *Doin et al.* [1997] where the heat flow was 15 mW m^{-2} and the chemical density contrast 60 kg m^{-3}. The entrainment rate from equation (38) is 100 km Gyr^{-1} compared with 120 km Gyr^{-1} in their two-dimensional numerical model. This indicates that the scaling in equation (38) gives reasonable estimates for the entrainment rate.

3.4.2. Entrainment of Very Viscous Chemical Lithosphere

[111] *Doin et al.* [1997] note the difficulty of rapid entrainment and suggest that the chemical lithosphere is too viscous to readily flow into the cusps to be entrained. I now find when the viscosity contrast, η_C/η_0 becomes large enough to retard entrainment.

[112] I begin by noting that I obtained the scaling relationship (38) between heat flow and entrainment by considering the flow balance around wisps of entrained material. I presumed that the chemically buoyant lithosphere was able to flow laterally toward the cusps where it could be entrained. This assumption is invalid if the chemical lithosphere is much more viscous than normal mantle. I obtain the dimensional scaling for this case considering the horizontal flow of material in a boundary layer beneath very viscous rigid chemical lithosphere, that is, I approximate equation (11) as simple shear.

[113] I begin with flow within the boundary layer in the normal mantle (Figure 13). The thickness of this layer is dimensionally from equations (E5) and (E6):

$$\Delta Z_3 \approx Z_C \frac{\Delta T_3}{T_H}. \tag{39}$$

The material flux (velocity times thickness) through this layer is dimensionally

$$f_3 \approx \frac{\tau_V \Delta Z_3^2}{\eta_0}, \tag{40}$$

where the shear traction driving horizontal flow scales with the convective stress τ_V. Similarly, the entrained layer thickness in the chemical layer is dimensionally

$$\Delta Z_C \approx Z_C \frac{T_\eta}{T_H}. \tag{41}$$

The horizontal flux through this layer is

$$f_C \approx \frac{\tau_V \Delta Z_C^2}{\eta_C \exp\left(\Delta T_3/T_\eta\right)}, \tag{42}$$

where the exponential term represents that the interface is ΔT_3 cooler than normal mantle. The horizontally flowing layers eventually become part of downwellings. Conservation of mass implies that the heat flow (carried by downwellings) scales with the horizontal flux toward these downwellings

$$q \propto \rho C \Delta T_3 f_3, \tag{43}$$

and the thinning rate of the chemical layer scales with f_C. At quasi-steady state, this heat flow is equal to the conductive heat flow through the rigid lid in equation (E4) and the heat flow through the boundary layer in equation (E6). Combining equations (39)–(43) then yields the thinning rate of the lithosphere in terms of heat flow

$$-\frac{\partial Z_C}{\partial t} = \left[\frac{\eta_C}{\eta_0}\right]^{-1}\left[\frac{T_\eta}{\Delta T_3}\right]^2 (\rho C \Delta T_3)^{-1} \exp\left(-\Delta T_3/T_\eta\right) q_C, \quad (44)$$

where the heat flow is that of quasi-steady conduction through the chemical lithosphere q_C. This expression applies when the viscosity of the chemical layer limits its entrainment while equation (38) applies when the buoyancy of the layer limits entrainment. That is, the entrainment rate as a function of viscosity ratio is a constant from equation (38) below a critical ratio and inversely proportional to the ratio from equation (44) above that ratio. *Davaille et al.* [2002] obtained the dependence on viscosity ratio of entrainment by cylindrical plumes. By analogy to their work, the entrainment rate in two dimensions follows the proportionality

$$-\frac{\partial Z_C}{\partial T} \propto \left[\frac{\Delta \rho_C}{\rho \alpha \Delta T_3} + c\frac{\eta_C}{\eta_0}\right]^{-1}, \quad (45)$$

where C is a dimensionless parameter of order 1 that includes the exponential term in equation (44). This gives the limiting behaviors in equations (38) and (44) when one term is large compared with the other.

[114] The form in equation (44) is convenient when entrainment significantly thins the chemical lithosphere. The entrainment rate increases with lithospheric thinning as q_C increases. Eventually, the chemical lid becomes thin enough that $q_C \approx q_S$, and a thin stable lid becomes established.

[115] The exponential term in equation (44) is of order 1 from equation (E4) $q_S \gg q_C$. Conversely, equation (44) then does not depend strongly on the precise form of equation (E4). The exponential term is significant for when $q_S \approx q_C$ in equation (E4) and entrainment is sluggish.

[116] I now manipulate equation (44) into a form where the long-term history of gradual entrainment is more evident. I equate the heat flows in equations (E4) and (E6) and drop the exponential term to eliminate ΔT_3,

$$-\frac{\partial Z_C}{\partial t} \approx \left[\frac{\eta_C}{\eta_0}\right]^{-1} \left(\rho C T_\eta\right)^{-1} q_C^{-5/4} q_S^{9/4}. \quad (46)$$

The heat flow q_S is the most strongly temperature-dependent term in equation (46). Using equation (12) for the heat flow q_S and equation (7) for the viscosity yields the proportionality for the past entrainment rate in terms of the modern one

$$\left[-\frac{\partial Z_C}{\partial T}\right]_R \propto T_\eta^{-1} \exp\left[\frac{3\Delta T_R}{4T_\eta}\right]\left[\frac{-\partial Z_C}{\partial T}\right]_{\text{now}}, \quad (47)$$

where ΔT_R temperature difference between the past mantle adiabat and the modern one.

[117] Equations (46) and (47) are convenient (for successful cases) when the chemical lithosphere is slowly entrained so that its thickness and heat flow q_C do not change much. Then, a strongly temperature-dependent viscosity aids entrainment particularly in the past when the mantle was hotter. For example, a 150 K higher temperature with $T_\eta = 43$ K implies that the past rate of entrainment was 13 times the modern rate. (Note that episodes of enhanced entrainment rate should occur when hot plume material transiently underplates the lithosphere.)

3.4.3. Numerical Model With Chemically Buoyant Lithosphere

[118] I obtained scaling relationships for entrainment of chemical lithosphere (equations (38) and (46)). I present model C1 to spot check, calibrate, and illustrate my scaling results.

[119] As in the scaling relationships, I assume a linear nondepth-dependent rheology and define the properties of chemically buoyant lithosphere with its density and viscosity contrast. I vary the ratio η_C/η_0 to find minimum values compatible with long-lived cratonal lithosphere.

[120] I assume a simple hot starting condition. At 3200 Ma, a 60-km-thick conductive layer overlies an adiabatic half-space. The flat base of the chemical layer is at 192.5-km depth (the grid centered at 190-km depth). The models are sufficient to resolve the cusps at downwellings within the normal mantle and upwellings within the chemical lithosphere. That is, they resolve the amount of entrainment and the vigor of convection. They do not resolve the details of wisps once they are entrained. The effect of numerical dispersion is to increase the computed amount of entrainment over that which would occur in nature.

[121] I limit models to those where the modern q_S is 24 or 52 mW m^{-2}. The former heat flow is comparable to the mantle heat flow through cratons. It implies that the quasi-steady lithospheric thickness beneath platforms where no chemical layer exists is comparable to that of cratons where the chemical layer is present. The latter heat flow is that of old ocean basins. This is the situation envisioned by *Davaille and Jaupart* [1994] and *Doin et al.* [1997] where localized convection supplies the heat flow through old oceanic lithosphere. I restrict T_η to the plausible values of 43 K and 100 K.

[122] I present model C1 models in the physically likely range where the thickness of the chemical layer does not change a lot over time. It has $T_\eta = 100$ K, $\eta_C/\eta_0 = 10$, and $\eta_0 = 0.28 \times 10^{20}$ Pa s. The current half-space heat flow q_S is 24 mW m^{-2}. The 5-km numerical grid resolves the scale thickness $\Delta Z_C \sim 15$ km of the entrained chemical layer in equation (41). The two-dimensional box controls the details of the planform. Basal shear in the Earth would reorganize cusps after changes in plate motion. Conversely, relief at the base of the chemical lithosphere should modulate the planform of convection and act as catchments for ponded plume material.

[123] I first appraise the predicted inverse dependence of entrainment rate on η_C/η_0 in equation (46). I let this parameter be 10 (model C1), 20, and 40 and keep the other parameters constant. Entrainment in the first 800 Myr of the models with $\eta_C/\eta_0 = 10$, 20, 40 is an equivalent thickness of 14, 8, and 5 km, respectively, that is, crudely the expected inverse dependence.

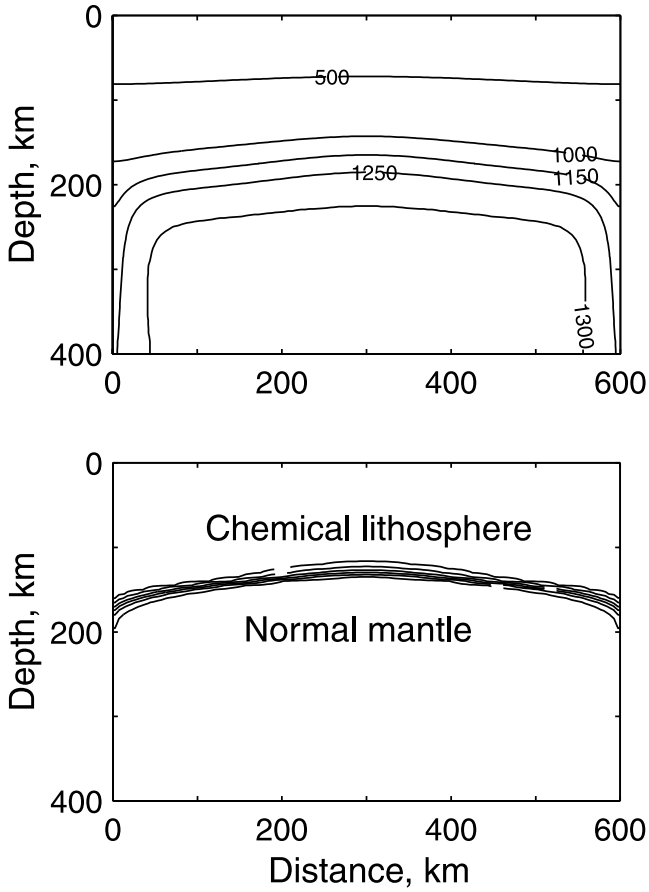

Figure 14. (top) Present potential temperature and (bottom) lithospheric component shown for model C1. The interface has pronounced cusps at the sides of the box and is shallower than its original depth of 192.5 km.

[124] To appraise the dependence of entrainment on q_S in equation (46), I compute a model where the modern heat flow q_S is 52 mW m^{-2} ($\eta_0 = 0.28 \times 10^{19}$ and the parameters from model C1). Equation (46) predicts that the entrainment rate is $10^{3/4} = 5.6$ times that of model C1 for the same viscosity ratio. As expected from this, entrainment removes an excessive amount of the chemical lithosphere in the model with $\eta_C/\eta_0 = 10$. More usefully, the predicted entrainment rate is 5.6/5 that of model C1 (16 km) for $\eta_C/\eta_0 = 50$. This viscosity ratio is greater than the ratio (<25) between depleted mantle and normal mantle determined by *Doin et al.* [1997] by considering mineral physics and also noting that xenoliths indicate that cratonal mantle has undergone some metasomatism with components that should decrease its viscosity. The computed entrainment for that model in the first 800 Myr is an equivalent thickness of 24 km, somewhat higher than the prediction of 16 km scaling from model C1.

[125] I did not numerically check the predicted dependence on T_η in equation (47) for $T_\eta = 43$ K when the mantle was 150 K hotter because my grid is too coarse. Instead, I use equation (47) to find for modern q_S is 24 mW m^{-2} that η_C/η_0 needs to be a factor of 10 greater than that in model C1 (100) for a similar amount entrainment, which is excessive.

[126] I present the results of the model C1 with $\eta_C/\eta_0 = 10$ and $\eta_0 = 0.28 \times 10^{20}$ Pa s in more detail because there is enough entrainment that its effects are evident. The lithospheric thickness, once stabilized, decreases slowly over time as entrainment thins the chemical lithosphere (Figure 5). The tendency of convection within the normal mantle to wane over time as it cools counteracts this effect to some extent.

[127] Entrainment thins the chemical layer by an equivalent thickness of 48 km over the life of model C1. The remaining chemical layer still affects convection, but the top rheological boundary layer and the base of the chemical layer are too shallow (~140 km) to provide a source region for unsheared depleted xenoliths down to ~180 km depth (Figure 14). I use the linear scaling with respect to viscosity ratio in equation (46) to get an improved model based on model C1 with I adjust the initial thickness of the chemical layer to obtain the modern measured thickness (~180 km). For example, a model similar to model C1 needs an initial chemical lithosphere thickness of ~228 km to allow for ~48 km of entrainment. More reasonably, a model with a viscosity ratio of 20 needs an initial thickness of ~204 km to allow for ~24 km of entrainment. This is my preferred model as the viscosity ratio is within the range given by *Doin et al.* [1997].

[128] To summarize, the buoyancy of cratonal lithosphere alone is not an effective impediment to its entrainment. For any reasonable convective heat flow q_C through the chemical lithosphere, density-limited entrainment in equation (38) is fast, ~100 km Gyr^{-1}. The chemical layer from equation (46) thins slowly if it is much more viscous then normal mantle, particularly if viscosity is not strongly temperature-dependent ($T_\eta = 100$ K). The dependence of entrainment rate in equations (46) and (47) on the temperature of the normal mantle indicates that the high temperatures in the past need to be explicitly considered in modeling cratonal stability. The preferred model has the modern stagnant lid convective heat flow q_S similar to the conductive heat flow q_C. This provides a heat flow ~q_S to younger platform regions that presumably lack thick buoyant lithosphere and is compatible with the observation that platform lithosphere is almost as thick as cratonal lithosphere.

4. Discussion and Conclusions

[129] The straightforward interpretation of xenolith data is that the lithospheric thickness (defined as the depth where the extrapolated conductive geotherm intersects the mantle adiabat) is between 200 and 250 km for large cratons. The xenolith data indicate that cratonal lithosphere approached its modern thickness soon after the cratons stabilized and that the cratonal lithosphere above ~180 km depth has remained stable since then. Sheared xenoliths and the xenolith geotherm constrain the temperature range across the rheologically active boundary layer to be <300 K. These inferences are compatible with the better resolved seismic and magnetotelluric studies, which do not provide more detailed constrains. The freeboard of the continents and the stress history of cratons provide limited confirmation that the thickness of cratonal lithosphere did not change much once they stabilized in the Archean.

[130] More information is potentially available from xenoliths. For example, the sheared xenoliths might be quantitatively related to strain rates, temperature, and time-dependent rheology in a self-consistent manner. Pressure-temperature-time paths would quantify the thinning or the thickening of the lithosphere over its history.

[131] The thickness of cratonal lithosphere, ~225 km, is small enough that is must be kept thin by convective heat transfer from the underlying mantle. In the absence of such convection, the lithosphere would be several hundred kilometers thick. Mantle plumes and basal drag on the thermal boundary layer from plate motions provide only a minor fraction of the heat flow from the underlying mantle. This leaves localized convention as the likely mechanism. This convection must have functioned in a way that cratonal lithosphere was stabilized in the Archean and remained stable.

[132] A common explanation for the longevity of cratonal lithosphere is that it is chemically buoyant relative to the underlying normal mantle. The buoyant layer then acted as a lid to the underlying convection, maintaining nearly constant lithospheric thickness over time. This hypothesis is viable but requires that the chemical layer did not become entrained into the underlying convection. Buoyancy alone in equation (38) is an ineffective deterrent to entrainment. The chemical lithosphere needs to be significantly more viscous (at given conditions) then the underlying mantle to remain stable. Weakly temperature-dependent viscosity in equations (46) and (47) retards entrainment. The entrainment rate in equation (46) scales as heat flow q_S from stagnant lid convection in the normal mantle equation (12) to the 9/4 power. The preferred ratio η_C/η_0 of the viscosity of the chemical layer in equation (7) to that of the normal mantle in equation (7) is ~20 for a temperature scale for viscosity T_η of 100 K and modern q_S similar to conductive heat flow q_C in equation (E6) through the chemical lid. Larger viscosity ratios are required if stagnant lid heat flow compatible to that through old oceanic lithosphere $q_S = 2q_C$ or if viscosity is strongly temperature-dependent (T_η = 43 K).

[133] Given that the Earth might not satisfy these restrictive conditions, it is conceivable that chemical buoyancy played a role in the initial stabilization of cratons but not their longevity. That is, stagnant lid convection in the normal mantle provides the heat flow to the lithosphere. A simple form of this hypothesis does not work if the mantle cooled significantly, ~150 K, since the Archean because the vigor of convection should wane over time and the lithospheric thickness in equation (9) should increase. The observed temperature range across the rheologically active boundary layer in equation (15) precludes very weakly temperature-dependent viscosity.

[134] I identify promising simple parts of parameter space where both the lithosphere thickens slowly with time and the temperature range across the rheological boundary layer is small from scaling relationships in Figures 3, 4, and 8. This yields two classes of models that involve strongly depth-dependent viscosity in different ways. I present dimensional analysis to appraise these classes and two numerical models for spot checking and illustration.

[135] In the first case, the viscosity decreases with depth along an adiabat. This decrease cannot continue to great depths but might occur owing to partial melt or metasomatism within the seismic low-velocity zone between ~120 and 220 km depth. The decrease in viscosity with depth then offsets the increase in viscosity with temperature as the Earth cooled in equation (17). Model L1 confirmed the behavior predicted from the dimensional analysis.

[136] In the second case, basal drag from plate motions dominates the stress invariant in equation (8). Localized convection aligned in rolls then behaves as if the fluid was linear. In this case, the temperature range across the thermal boundary layer in equation (15) is that for a linear fluid and the heat flow in equation (22) changes little as the mantle cools over time. However, dimensional scaling indicated that the basal drag in the Earth is not high enough for this pseudolinear limit to apply. The behavior for a large (but plausible) basal drag in model N1 is a mixture of the expected behavior for nonlinear convection and pseudolinear convection. That is, heat flow changes slowly over time as predicted by equation (22), but the temperature range across the rheological boundary layer is nearly as large as that for a nonlinear fluid is in equation (15).

[137] The restrictive nature of these somewhat successful models may indicate that the Earth is more complicated. In general, the rheology may be nonlinear, time-dependent, depth-dependent, and chemistry-dependent in a complicated way. Three-dimensional numerical models with plates and plumes would realistically represent the history of chemically buoyant lithosphere. One may explicitly consider metasomatism and renewal of chemical lithosphere. My compiled scaling relationships can be extended to some complex situations, but the bulky results would not be illuminating unless one began with insight into mantle rheology.

[138] For now, my scaling relationships and models then serve as a qualitative guide. For example, model N1 indicates that basal drag affects the stress invariant in nonlinear models. Models L1 and N1 indicate the possibility that the chemical buoyancy of cratonal lithosphere may not cause its longevity.

[139] Given this caveats, I prefer chemically buoyancy as the simplest means of keeping cratonal lithosphere stable since the Archean. A model with the parameters of model C1 except with chemical lithosphere viscosity factor of 20 more viscous than normal mantle allows only ~24 km of entrainment since the craton stabilized. The viscosity ratio is in the range expected by *Doin et al.* [1997]. Although I present no quantification, this relatively low viscosity ratio is attractive because chemical lithosphere deformed at the time of its formation and during subsequent metasomatic events.

Appendix A: Transient Cooling and Steady State

[140] I assumed that heat flow was quasi-steady in my scaling results. The thermal timescale of the lithosphere, several hundred million years, cannot be dismissed outright. I estimate the effects of transient cooling approximating the geotherm as linear in equation (9). I consider cooling of the mantle adiabat and gradual thickening of the lithosphere separately. My numerical calculations explicitly include these processes.

[141] I obtain the effect of transient cooling of the mantle adiabat as an equivalent heat flow using the linear geotherm in equation (9):

$$q_{\text{lith}} = \frac{\rho C Z_H}{2} \frac{\partial T_H}{\partial t}, \tag{A1}$$

where T_H is the potential temperature of the mantle adiabat. Assuming that the mantle adiabat cooled by 50 K Gyr^{-1}, $\rho C = 4 \times 10^6$ J m^{-3} K^{-1}, and that the lithosphere is 250 km thick yields a heat flow of 0.8 mW m^{-2}.

[142] Thickening of the lithosphere at constant basal temperature similarly produces an equivalent heat flow

$$q_t = \frac{\rho C T_H}{2} \frac{\partial Z_H}{\partial t}. \tag{A2}$$

For example, thickening of the lithosphere by 25 km Gyr^{-1} would produce a heat flow of 2 mW m^{-2} for a basal temperature of 1300°C. The sum of the two effects is 2.8 mW m^{-2}, which is small enough that the steady state assumption is tolerable in dimensional calculations.

Appendix B: Heat Transfer by Mantle Plumes

[143] Mantle plumes episodically impinge on the base of the lithosphere. The global average of heat flow from this process is ~7 mW m^{-2} [*Davies*, 1988; *Sleep*, 1990], less than half the mantle heat flow in cratons. The cratonal plume heat flow is probably less than the global average as modern hot spots are concentrated in the ocean basins. (A detection bias does exist.) Even when starting plume heads impinge on continental lithosphere, like within Africa, the buoyant plume material tends to pond beneath regions where the lithosphere is thin rather than beneath thick cratonal keels [*Sleep*, 1997; *Ebinger and Sleep*, 1998].

[144] Second, cratons where plumes have recently impinged should be thinner than average. This is true for the Tanzanian craton [*Chesley et al.*, 1999], but other examples are not evident.

[145] Third, plume impingement on cratons is to some extent a random process where more plumes impinge on some cratons than on others over lithospheric thermal timescale time of several hundred million years. Therefore the cratons receiving the most plumes are the thinnest. This is contrary to the observation that there is little variation in the lithospheric thicknesses of large cratons. For simplicity, I model this effect as a result from the statistics of small numbers.

[146] I begin with the long-term average heat flow from plumes to obtain an estimate of the rate at which plumes must impinge if they are to supply most of the heat flow into cratons. The plume heat flow is approximately

$$q_{\text{plume}} = \rho C \frac{\Delta T_{\text{plume}} Z_{\text{plume}}}{\Delta t_{\text{plume}}}, \tag{B1}$$

where plumes underplate the craton with a thickness Z_{plume} of material with an excess temperature above the mantle adiabat of ΔT_{plume} at an average time interval of Δt_{plume}. Frequent thick plume layers are needed to supply much of the cratonal heat flow. For example, twice the global average plume heat flow, 13.5 mW m^{-2}, is supplied for $\Delta T_{\text{plume}} = 200$ K, $\rho C = 4 \times 10^6$ J m^{-3} K^{-1}. $\Delta t_{\text{plume}} = 75$ Myr, and $Z_{\text{plume}} = 40$ km.

[147] Returning to statistical vagaries, I estimate the expected range in cratonal thickness by assuming that plumes impinge on average every 75 Myr over the effective thermal time constant of the lithosphere of 450 Myr, yielding six plume events. The expected range in this number is crudely $\sqrt{6} \approx 2.45$, which implies a ±40% relative scatter about the mean heat flow and mean lithosphere thickness.

[148] That is, for plumes to provide the bulk of the heat flow beneath cratons, they must target these regions more frequently than average for the Earth's surface and do so in a temporally and spatially regular manner. There is no evidence that plumes behave in this way.

Appendix C: Heat Transfer by Basal Drag

[149] Cratonal lithosphere moves with respect to the underlying mantle. Basal drag tends to displace the basal boundary layer and replace it with hotter mantle from the surrounding regions of thin lithosphere. The process is analogous to speeding heat transfer by fanning a surface.

[150] I obtain a dimensional scaling for the heat flow associated with basal drag by representing the lithosphere in a two-dimensional cross section from somewhere within a craton to a ridge axis where the lithosphere is quite thin and the geotherm is the mantle adiabat. I consider the process to be quasi-steady state with the only change being the slow cooling of the mantle adiabat with time.

[151] I obtain the heat flow from basal drag q_b by considering the local balance between conductive heat loss to the surface and heat carried within the thermal boundary layer with a region of the cross section (Figure C1). To do this, I solve the momentum equation (11) by approximating the flow beneath the craton as horizontal simple shear driven by (vertically) constant shear traction τ_D. That is, I apply lubrication theory. For simplicity, I assume that viscosity depends on temperature but not explicitly on depth within the boundary layer. The (simple shear) strain rate within the boundary layer (for both linear and nonlinear rheology) is from equations (7) and (8)

$$\varepsilon' = \frac{\tau_D}{\eta_0} \exp\left[\frac{-\Delta T}{T_\eta}\right], \tag{C1}$$

where without loss of generality the reference shear traction is τ_D and ΔT the temperature below the mantle adiabat. The geothermal gradient within the boundary layer scales with the conductive geothermal gradient within the lithosphere T_H/Z_H. Then the strain rate decays upward into the boundary layer over a dimensional depth scale of

$$\Delta Z_{\text{rheo}} = Z_H \frac{T_\eta}{T_H}. \tag{C2}$$

The horizontal velocity within the boundary layer relative to the craton is the integral over depth of the strain rate, which also decays upward over a depth scaling dimen-

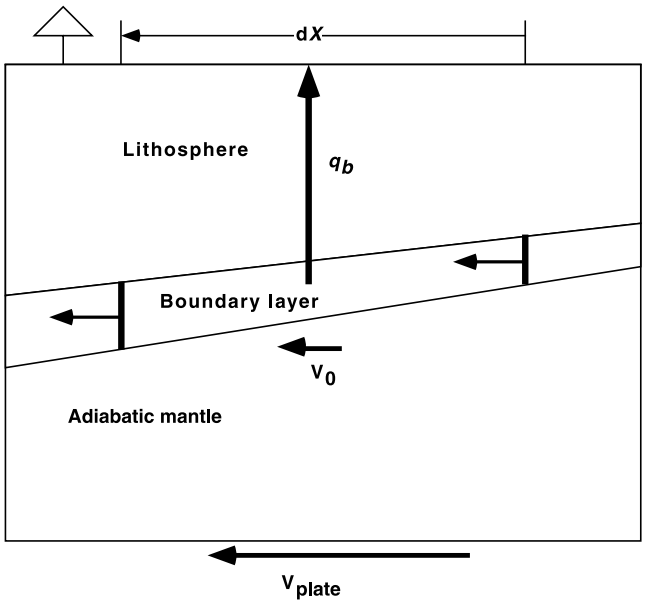

Figure C1. Heat balance on a grid of lithosphere of width dX. The coordinate system is relative to fixed lithosphere. The velocity at the base of the rheologically active boundary layer V_0 is a fraction of the plate velocity V_{plate}. The thickness of the rheologically active boundary layer scales with the overlying lithospheric thickness. The layer thickens down stream so that it carries less heat out of the grid than came in. The heat flow q_b transports this heat to the surface.

sional with ΔZ_{rheo}. The velocity at the base of the boundary layer is then dimensionally

$$V_0 \approx \frac{\tau_D \Delta Z_{\text{rheo}}}{\eta_0} = \frac{\tau_D Z_H T_\eta}{\eta_0 T_H}. \quad \text{(C3)}$$

This result is kinematically equivalent to that which would be obtained from an equivalent layer of thickness Z_{rheo} and the viscosity (here η_0) at the base of the boundary layer. The velocity at the base of the thermal boundary layer V_0 scales with the plate velocity V_{plate} (Figure C1). Again solving equation (11) assuming simple shear and considering depth-dependent viscosity of the underlying mantle explicitly, velocity of the base of the boundary layer relative to deep mantle is

$$V_{\text{plate}} - V_0 = \int_{Z_H}^{z} \frac{\tau_D}{\eta_0} \exp\left[\frac{-Z}{D_\eta}\right] dZ \approx \frac{\tau_D D_\eta}{\eta_0} \exp\left[\frac{-Z_H}{D_\eta}\right], \quad \text{(C4)}$$

where Z is a dummy variable for depth and the upper limit of the integral is taken as infinity in the second inequality. This simple shear velocity is that of an equivalent layer of thickness D_η and the viscosity at the base of the boundary layer. The fraction of the plate velocity that acts to drag the boundary layer is

$$\frac{V_0}{V_{\text{plate}}} \approx \frac{\Delta Z_{\text{rheo}}}{\Delta Z_{\text{rheo}} + D_\eta}. \quad \text{(C5)}$$

This result is depends only on the relative variation of viscosity with depth.

[152] I solve the heat flow equation (10) by conserving energy at steady state within a region of width dX. The surface heat loss from the region is $q_b dX$. The horizontal (volume per length) flux within the boundary layer is dimensionally $V_0 \Delta Z_{\text{rheo}}$, and this material is, on average, a temperature scaling with T_η less than the mantle adiabat. This implies that drag within the boundary layer carries heat into and out of the region, which scales with $\rho C T_\eta V_0 \Delta Z_{\text{rheo}}$. The heat balance is dimensionally, using equation (C3),

$$q_b = k\frac{T_H}{Z_H} \approx \frac{d}{dX}\left[\frac{\rho C V_0 Z_H T_\eta^2}{T_H}\right] = \left[\frac{\rho C V_0 T_\eta^2}{T_H}\right]\frac{dZ_H}{dX}, \quad \text{(C6)}$$

where I remove parameters considered constant from the derivative in the second equality.

[153] I obtain the steady state dimensional solution by integrating equation (C6) from a ridge axis (where the lithospheric thickness is zero) to the point in the craton. This yields

$$Z_H \approx \frac{T_H}{T_\eta}\left[\frac{2\kappa X}{V_0}\right]^{1/2}, \quad \text{(C7)}$$

where X is the distance from the ridge axis. This result has the attractive feature that through equation (C4) it depends only on the relative variation of viscosity with depth. That is, it predicts that the quasi-steady lithosphere thickness changes little as the Earth's mantle cooled and became more viscous. The heat flow is dimensionally

$$q_b = k\frac{T_H}{Z_H} \approx kT_\eta\left[\frac{2\kappa X}{V_0}\right]^{-1/2}. \quad \text{(C8)}$$

There is a simple geometrical interpretation of this expression. Flow replaces the boundary layer on a scale time X/V_0. Equation (C8) then has dimensional form of the heat flow out of a half-space, where the boundary temperature differs from the interior temperature by T_η.

[154] I appraise whether basal drag is a viable mechanism for supplying most of the heat flow to cratons beginning with the inference from xenoliths that temperature contrast across the rheological boundary layer is <300 K. In analogy with equation (15), the temperature range is $\sim 2T_\eta$, implying that $T_\eta < 150$ K.

[155] This limit $T_\eta = 150$ K constrains D_η as this parameter from equation (C5) needs to be comparable or smaller than the rheological layer thickness for significant drag to occur within the boundary layer. I quantify this inference letting that the actual rheological boundary layer thickness be twice that in equation (C2) in analogy with equation (16). Plausible values of $T_H = 1300°C$, $Z_H = 200$ km, and $V_0/V_{\text{plate}} = 0.5$ give $D_\eta = 46$ km (or a little less than an order of magnitude per 100 km).

[156] This difficulty is severe if mantle viscosity is in fact strongly temperature-dependent. For example, a change of 1 order of magnitude of viscosity over 100 K ($T_\eta = 43$ K) is a venerable approximation. The velocity V_0 is then half the plate velocity when $D_\eta = 13$ km, implying over 3 orders of magnitude change over 100-km depth.

[157] I continue with the observed quantity that basal drag might supply, mantle heat flow. I use $T_\eta = 150$ K and

equation (C8) to obtain an upper limit for heat flow for a wide craton. The width X is strictly the distance to the nearest ridge axis in the direction of plate motion. It is clearly more that the width of a craton, which is difficult to define precisely. Maps by *Haggerty* [1999] and by *Artemieva and Mooney* [2001] indicate that the Canadian Shield is over 2000 km across. Using this width, $V_0 = 0.5 \times 10^{-9}$ m s^{-1}, $\kappa = 0.75 \times 10^{-6}$ m^2 s^{-1}, $D_\eta = 46$ km, and $k = 3$ W m^{-1} K^{-1} yields a heat flow of 5.7 mW m^{-2}.

[158] This is only a moderate amount of observed cratonal heat flow, but some caution is mandated because equation (C8) is a dimensional result. The numerical models of *Lenardic and Moresi* [2000] provide confirmation and calibration of the inference that basal drag is not the dominant heat flow mechanism beneath wide cratons. In their models, T_η is ~160 K and the effective width of their craton (from edge to major downwelling driving flow) is only 500 km.

[159] An additional problem with basal drag is that cratonal lithospheric thickness should correlate with the square root of cratonal width and inversely with the square root of cratonal plate velocity. That is, one expects that the lithosphere of fast moving cratons, like India, to be thinner. (In this case, thinner lithosphere could be also attributed to the effect of plumes.) The width of cratons is a longer lasting difference than plate velocity. The narrow Tanzanian craton has thin lithosphere as expected from equation (C8) [*Chesley et al.*, 1999] but is also affected by ponded plume material. The width of larger cratons is not as easily defined (as noted just above). From *Haggerty*'s [1999] and *Artemieva and Mooney*'s [2001] maps, at least a factor of 2 variation exists between 700 km for the Guyana and South African cratons and over 1400 km for (only) the Laurentian part of the Canadian shield. The predicted $\sqrt{2}$ variation of lithospheric thickness between the Canadian shield and South Africa is not observed in the xenolith data [*Rudnick and Nyblade*, 1999], which indicates that any difference associated with width is much smaller.

[160] I conclude that basal drag does not likely supply most to the heat flow to the wider cratons. It may be significant for narrow cratons like Tanzania, but there are a too few well-studied examples to do phenomenology.

Appendix D: Two-Dimensional Numerical Methods

[161] I modify the numerical method for solving the momentum equation (11), heat flow, and chemical material flow equation (10) in two dimensions after *Andrews* [1972]. The in-plane flow from convection and antiplane flow from basal drag then separate in equation (11) except for the invariant in equation (8).

[162] For the in-plane flow, I take the curl of equation (11) to eliminate pressure. This yields an equation for the stream function, which is the biharmonic equation $\nabla^4\psi = 0$ for contrast viscosity and density. I solve for the stream function at each time step (for variable viscosity and thermal and chemical density contrasts) by overrelaxation.

[163] I define the antiplane flow in terms of the antiplane velocity. Equation (11) then reduces to LaPlace's equation $\nabla^2 V_y = 0$ for constant viscosity. I also solve this equation for variable viscosity by overrelaxation.

[164] The models have a uniform 5-km square grid with 600-km horizontal and 400-km vertical dimensions. I define temperature, chemical component, and antiplane velocity at nodes in the middle of the grid defined by the stream function nodes. I obtain the strain rate invariant to evaluate nonlinear viscosity at the stream function nodes.

[165] I modify *Andrews'* [1972] approach by using overrelaxation to obtain the stream function and by using the upstream temperatures rather than extrapolated temperatures halfway through the time step to solve for the divergence of the product of velocity and temperature. The former modification allows nonlinear viscosity to be included. The latter conserves energy, as did *Andrews'* [1972] formulation, and helps maintain numerical stability.

[166] I start the calculations with a linear thermal gradient above an adiabatic interior. I obtain the starting antiplane velocity by solving the one-dimensional simple shear problem. I set the starting stream function to zero at all nodes. I perturb the temperature with zero mean at all nodes at a given depth, 40 km, within the boundary layer. The eventual quasi-steady state, not the details of the start up, is the object of the calculations.

[167] These starting and boundary conditions allow overrelaxation to work effectively. It is necessary to represent the thermal structure near the boundary layer accurately (and to conserve energy in the downwellings) to obtain the amount of heat transferred by convection. Short-wavelength variations in the stream function, which are important within the boundary layer, converge quickly by overrelaxation. Long-wavelength variations, which are less efficiently obtained, are strongly damped by the rigid region immediately above the boundary layer. The antiplane velocity changes little from the initial one-dimensional estimate. I checked its convergence by seeing if the laterally averaged shear traction at the top of the model balanced that at the bottom.

Appendix E: Two-Layer Convection Involving Buoyant Lithosphere

[168] Entrainment of normal mantle into the chemical lithosphere would reduce the chemical density contrast and cause the chemical lithosphere to be efficiently entrained into the underlying fluid. This process would have occurred rapidly if the chemical layer were sufficiently fluid that it convected internally. In that case, equation (38) dimensionally applies to entrainment of normal mantle into convection within the overlying chemical layer [*Sleep*, 1988]. Then a lower viscosity of the normal mantle relative to chemical lithosphere allows wisps to drain back into cusps. The effect, however, is small within two-dimensional upwellings for the expected chemical viscosity contrasts of a factor of ~10.

[169] I obtain dimensional relationships for steady state convection through a chemically buoyant layer overlying a half-space in analogy to the global layered models of *Butler and Peltier* [2002]. Three boundary layers exist for vigorous convection (Figure E1). From the top down, (1) a stagnant lid boundary layer is at the top of the convecting part of the chemical layer; (2) a boundary layer heated from below is at the base of the chemical layer; and (3) a more or less stagnant lid boundary layer is at the top of the ordinary

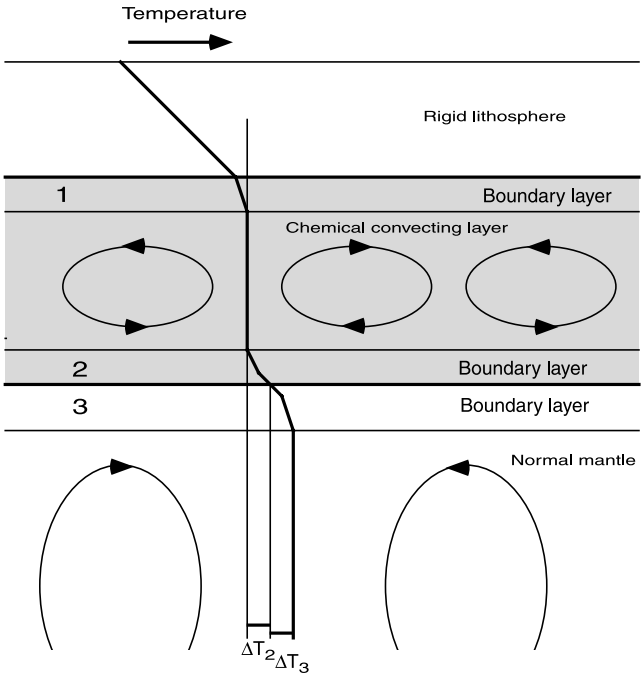

Figure E1. Schematic diagram of two-layer convection. At quasi-steady state, the conductive heat flow through the rigid lithosphere is equal to the convective heat flow through the two boundary layers in the chemically less dense region and the upper boundary layer in the normal mantle. The interior of the chemical layer and the normal mantle beneath the boundary layer are adiabatic. See text.

mantle. I let the temperature range across the latter two layers be ΔT_2 and ΔT_3, respectively. I denote the quasi-steady heat flow that would occur in ordinary mantle in the absence of a chemical layer in equation (12) using the viscosity in equation (7) by q_S.

[170] At quasi-steady state, the laterally averaged heat flow is the same for all three boundary layers. The upper layer is the simplest as it is basically stagnant lid convection. From equation (12) using the viscosity in equation (7), the heat flow through this layer is

$$q = \left[\frac{\eta_C}{\eta_0}\right]^{-1/3} \exp\left[\frac{-(\Delta T_2 + \Delta T_3)}{3T_\eta}\right] q_s. \tag{E1}$$

The magnitude of the temperature contrasts ΔT_2 and ΔT_3 is not obvious, but it is clear that it is not zero. This implies that the heat flow through the two-layer convection is less than q_S if the chemical layer is at least as viscous as ordinary mantle at given temperature.

[171] The second boundary layer is analogous to the boundary layer at the base of the mantle in that it is convection within a fluid with strongly temperature-dependent viscosity that is heated from below. Following *Christensen* [1984] and *Sleep* [1988], I represent effective viscosity as a weighted geometrical average of the viscosity of the chemical layer at its interface with the ordinary mantle and the viscosity within the adiabatic interior of the chemical layer:

$$\eta_2 = \eta_C \exp\left[\frac{0.3\Delta T_3}{T_\eta}\right] \exp\left[\frac{0.7(\Delta T_2 + \Delta T_3)}{T_\eta}\right], \tag{E2}$$

where the coefficients 0.3 and 0.7 result from a (log-log) linear fit to the heat flow versus viscosity curve in Figure 4 of *Christensen* [1984]. The heat flow through this boundary layer (using that figure to calibrate the multiplicative factor to 0.24) is

$$q = \left[\frac{0.24}{0.47}\right] \left[\frac{\eta_C}{\eta_0}\right]^{-1/3} \left[\frac{\Delta T_2}{T_\eta}\right]^{4/3} \exp\left[\frac{-0.3\Delta T_3}{3T_\eta}\right] \cdot \exp\left[\frac{-0.7(\Delta T_2 + \Delta T_3)}{3T_\eta}\right] q_S. \tag{E3}$$

The heat flow through the upper boundary layer in the normal mantle should depend on the temperature contrast across the boundary layer ΔT_3. This quantity cannot be zero as then no heat would be transmitted. It must be less than $2.4T_\eta$, the boundary layer thickness in equation (15) for stagnant lid convection that is unaffected by a chemical layer. The simplest form that preserves the dimensionality of the parameterized convection equation (12) and the stagnant lid limit is

$$q = \left[\frac{\Delta T_3}{2.4T_\eta}\right]^{4/3} q_S. \tag{E4}$$

Equation (E4) applies as an estimate both when the chemical layer is convecting and when it is more or less rigid.

[172] At quasi-steady state, the heat flows through the three boundary layers are equal. This results in three equations with three unknowns: the heat flow q and the boundary layer temperature ranges ΔT_2 and ΔT_3. The ratio of the temperature contrasts is independent of the heat flow q_S and their magnitude scales with T_η. The temperature range ΔT_2 is $1.48T_\eta$ independent of the viscosity contrast. This amount is not in gross error. *Solomatov and Moresi* [2002] give a preferred range of $1.1-1.3T_\eta$ for the related case of secondary convection within D″. The temperature contrast ΔT_3 and the ratio q/q_S decrease with the viscosity ratio η_C/η_0 (Figure E2). I expect that this behavior is fairly

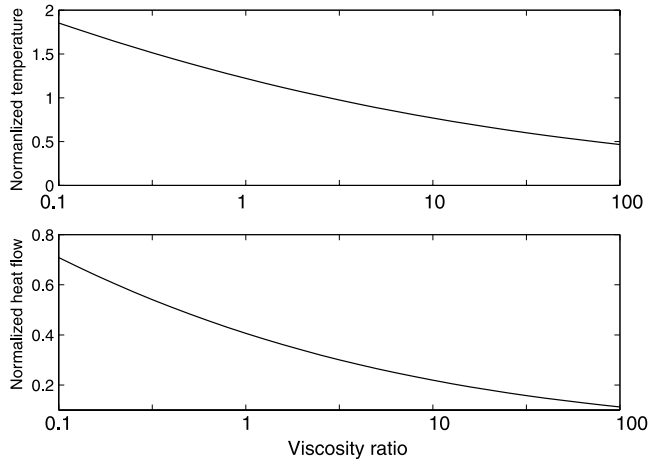

Figure E2. Properties of vigorous two-layer convection as functions of the viscosity ratio η_C/η_0. (top) Normalized temperature contrast is $\Delta T_3/T_\eta$ across the upper boundary layer in the normal mantle decreases with the viscosity ratio. (bottom) Quasi-steady heat flow is normalized to the stagnant lid heat flow q_S.

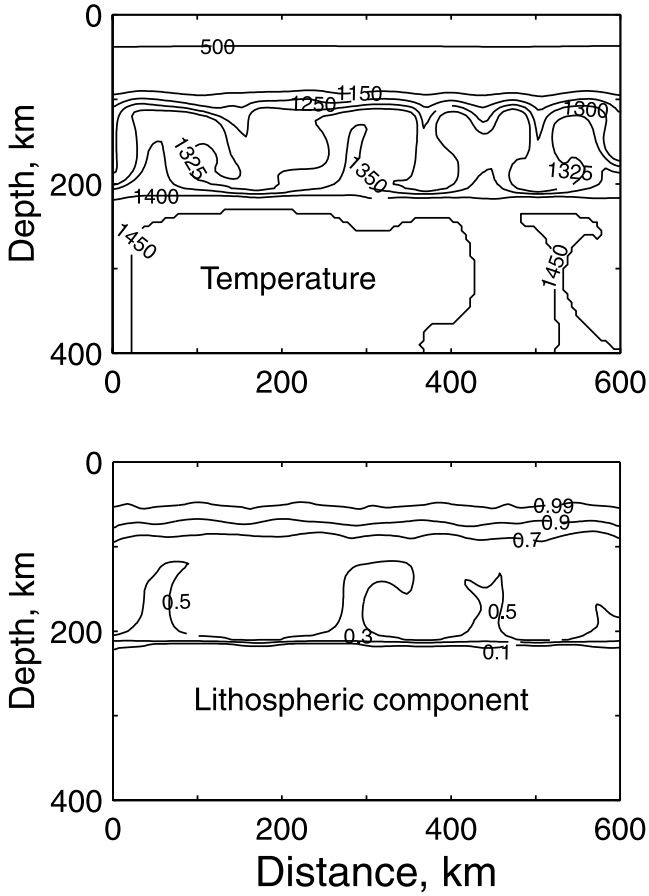

Figure E3. (top) Potential temperature and (bottom) lithospheric component for model T1 at 3000 Ma. Two-layer convection is well developed at the interface between the chemical boundary layer and the normal mantle. The chemical boundary layer by this time is a mixture of the original chemical layer and normal entrained mantle. The interface has moved downward from its initial depth of 192.5 km.

robust as it depends only on the dimensional form of the equations for heat flow in equations (E1), (E3), and (E4). That is, the heat flow depends on viscosity to the $-1/3$ power and the temperature contrast across the boundary layer to the 4/3 power. The precise results depend on the multiplicative coefficients in these equations, which are less well constrained.

[173] This purpose here is to see when two-layer convection can occur as this process leads to rapid entrainment. To obtain quick results, I note that heat flow in Figure E2 (where the chemical layer as least as viscous as normal mantle) is approximately

$$q = 0.406\left[\frac{\eta_C}{\eta_0}\right]^{-0.28} q_S. \tag{E5}$$

I compare this with the heat flow that would occur if the chemical layer acted as a rigid lid to convection in the underlying mantle

$$q_C \equiv \frac{kT_H}{Z_C}, \tag{E6}$$

where Z_C is the depth to the base of the chemical layer. The behavior of the convection once quasi-steady state is reached depends on the relative magnitudes of the heat flow associated with stagnant lid convection within the normal mantle q_S, the conductive heat flow through a rigid chemical layer q_C, and the heat flow through two-layer convection q. Two-layer convection occurs when q is significantly greater than q_C. Otherwise, convection capped by a more or less rigid chemical layer occurs when $q_S > q_C$. If this condition is not satisfied the thermal boundary layer in the normal mantle is fully beneath the chemical layer and the chemical layer has no effect on the quasi-steady heat flow as I assumed in section 3.3.

[174] The transient behavior on starting from a thin lithosphere over hot adiabatic mantle is more complicated. Initially, the thermal boundary layer is at the base of a lid made of chemical lithosphere. Stagnant lid convection begins within this boundary layer if it is not too viscous. Cool downwelling material from the stagnant lid ponds above the interface between the chemical lithosphere and normal mantle. This cooler material then triggers convection within the normal mantle. Convecting part of the

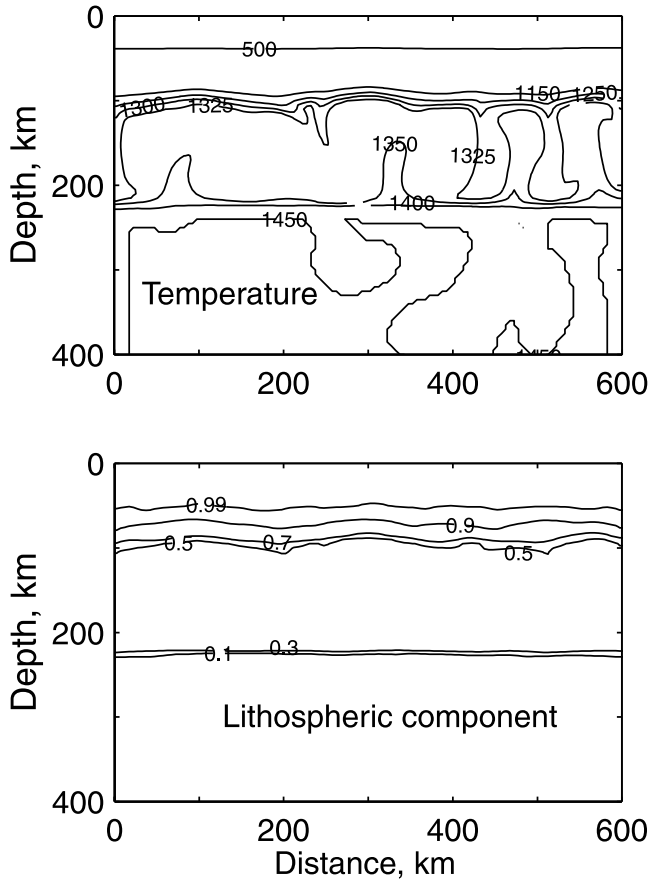

Figure E4. (top) Potential temperature and (bottom) lithospheric component for model T2 at 3000 Ma. Two-layer convection is well developed at the interface between the chemical boundary layer and the normal mantle. The chemical boundary layer by this time is a mixture of the original chemical layer and more than half entrained normal mantle. The interface has moved significantly downward from its initial depth of 192.5 km.

chemical layer cools until it either becomes rigid or reaches the temperature for two-layer convection. Entrainment in both directions occurs during this transient convection within the thermal boundary layer.

[175] I present a model T1 where the viscosity ratio $\eta_C/\eta_0 = 1$ to appraise the scaling relationships two-layer convection and illustrate the above paragraph (Figure E3). I let the viscosity be strongly temperature-dependent with $T_\eta = 43$ K and $\eta_0 = 10^{18}$ Pa s, so that the mantle is initially quite fluid. By 200 Myr after the start of the model, two-layer convection is well developed. The half-space heat flow q_S at this time is 75 mW m^{-2}. The current half-space heat flow is 24 mW m^{-2}, not much greater than the actual mantle heat flow through cratons. The expected heat flow from Figure E2 is 30.4 mW m^{-2}. The model heat flow is 31.2 mW m^2. The predicted temperature contrasts ΔT_2 and ΔT_3 are 64 K and 52 K, respectively, compared with the model amounts of ~75 K and ~50 K.

[176] Significant entrainment has already occurred by the time in Figure E3. The fraction of chemical lithosphere within the chemical layer decreased from 1 to ~0.55, and the interface has moved downward some indicating that entrainment of normal mantle into the chemical layer is somewhat faster than the other way around. The instantaneous entrainment rate from equation (38) is 250 km Gyr^{-1} compared with the model rate of 280 km Gyr^{-1}.

[177] I begin to investigate the effect of a more viscous chemical layer by increasing η_C/η_0 to 10 and decreasing η_0 to 10^{17} Pa s, in model T2 (Figure E4). By the time in Figure E4, entrainment of normal mantle into the chemical layer has reduced the chemical fraction to 0.45 and the viscosity ratio to 2.8. The predicted heat flow is 0.31 times the half-space heat flow of q_S = 161 mW m^{-2} or 50 mW m^{-2}. The model heat flow is somewhat lower, i.e., 43 mW m^{-2}. The predicted temperature contrasts ΔT_2 and ΔT_3 are 64 K and 43 K, respectively, compared with ~65 K and ~50 K in the model. The predicted entrainment rate is 350 km Gyr^{-1}, compared with 360 km Gyr^{-1} in the model.

[178] The scaling relationships give reasonable predictions for models T1 and T2. In practice, the main objective of the prediction is to avoid model parameters that imply an early demise of the chemical lithosphere that I assume to have been present at 3.2 Ga.

[179] Vigorous two-layer convection is unnecessary for rapid entrainment. The model lithosphere thinned by several tens of kilometers in the Archean for models where the modern q_S is 24 mW m^{-2}. These include $\eta_C/\eta_0 = 10$, T_η = 43 K, and $\eta_0 = 10^{18}$ Pa s and $\eta_C/\eta_0 = 1$, $T_\eta = 100$ K, and $\eta_0 = 0.28 \times 10^{20}$ Pa s.

[180] **Acknowledgments.** This research was in part supported by NSF grants EAR-9902079 and EAR-0000743. I thank George Thompson and three anonymous reviewers for helpful comments.

References

Abbott, D. L., L. Burgess, J. Longhi, and W. H. F. Smith, An empirical thermal history of the Earth's upper mantle, *J. Geophys. Res.*, *99*, 13,835–13,850, 1994.

Abbott, D. H., R. Drury, and W. D. Mooney, Continents as lithological icebergs: The importance of lithospheric roots, *Earth Planet. Sci. Lett.*, *149*, 15–27, 1997.

Anderson, D. L., and J. Polet, Depth extent of cratons as inferred from tomographic studies, *Geology*, *23*, 205–208, 1995.

Andrews, D. J., Numerical simulation of sea floor spreading, *J. Geophys. Res.*, *77*, 6470–6481, 1972.

Artemieva, I. M., and W. D. Mooney, Thermal thickness and evolution of Precambrian lithosphere: A global study, *J. Geophys. Res.*, *106*, 16,387–16,414, 2001.

Bank, C. G., M. G. Bostock, R. M. Ellis, Z. Hajnal, and J. C. VanDecar, Lithospheric mantle structure beneath the trans-Hudson orogen and the origin of diamondiferous kimberlites, *J. Geophys. Res.*, *103*, 10,103–10,114, 1998.

Bickle, M. J., Implications of melting for stabilization of the lithosphere and heat loss in the Archean, *Earth Planet. Sci. Lett.*, *80*, 314–324, 1986.

Boyd, F. R., J. J. Gurney, and S. H. Richardson, Evidence for a 150–200 km thick Archean lithosphere from diamond inclusion thermobarometry, *Nature*, *315*, 387–389, 1985.

Burke, K., and W. S. F. Kidd, Were Archean continental geothermal gradients much steeper than those of today?, *Nature*, *272*, 240–241, 1978.

Butler, S. L., and W. R. Peltier, Thermal evolution of Earth: Models with time-dependent layering of mantle convection which satisfy the Urey ratio constrain, *J. Geophys. Res.*, *107*(B6), 2109, doi:10.1029/2000JB000018, 2002.

Carlson, R. W., D. G. Pearson, F. R. Boyd, S. B. Shirey, G. Irvine, A. H. Menzies, and J. J. Gurney, Re-Os systematics of lithosphere peridotites: Implications for lithosphere formation and preservation, in *The J. B. Dawson Volume*, edited by J. J. Gurney et al., pp. 117–124, Red Roof Design, Cape Town, South Africa, 1999.

Chesley, J. T., R. Rudnick, and C.-T. Lee, Re-Os systematics of mantle xenoliths from the East African Rift: Age, structure, and history of the Tanzanian craton, *Geochim. Cosmochim. Acta*, *63*, 1203–1217, 1999.

Christensen, U. R., Instability of a hot boundary layer and the initiation of thermo-chemical plumes, *Ann. Geophys.*, *2*, 311–320, 1984.

Davaille, A., and C. Jaupart, Thermal convection in lava lakes, *Geophys. Res. Lett.*, *20*, 1827–1830, 1993a.

Davaille, A., and C. Jaupart, Transient high-Rayleigh-number thermal convection with large viscosity variations, *J. Fluid Mech.*, *253*, 141–166, 1993b.

Davaille, A., and C. Jaupart, The onset of thermal convection in fluids with temperature-dependent viscosity: Application to the oceanic mantle, *J. Geophys. Res.*, *99*, 19,853–19,866, 1994.

Davaille, A., F. Girard, and M. Le Bars, How to anchor hot spots in a convecting mantle, *Earth Planet. Sci. Lett.*, *203*, 621–634, 2002.

Davies, G. F., Ocean bathymetry and mantle convection, 1, Large-scale flow and hotspots, *J. Geophys. Res.*, *93*, 10,467–10,480, 1988.

De Smet, J., A. P. Van den Berg, and N. J. Vlaar, Early formation and long-term stability of contients resulting from decompression melting in a convecting mantle, *Tectonophysics*, *322*, 19–33, 2000.

Doin, M.-P., L. Fleitout, and U. Christensen, Mantle convection and stability of depleted and undepleted continental lithosphere, *J. Geophys. Res.*, *102*, 2771–2787, 1997.

Dumoulin, C., M.-P. Doin, and L. Fleitout, Heat transport in stagnant lid convection with temperature- and depth-dependent Newtonian or non-Newtonian rheology, *J. Geophys. Res.*, *104*, 12,759–12,777, 1999.

Ebinger, C. J., and N. H. Sleep, Cenozoic magmatism throughout east Africa resulting from impact of a single plume, *Nature*, *395*, 788–791, 1998.

England, P., and M. Bickle, Continental thermal and tectonic regimes during the Archean, *J. Geol.*, *92*, 353–367, 1984.

Forte, A. M., and J. X. Mitrovica, Deep-mantle high-viscosity flow and thermochemical structure inferred from seismic and geodynamic data, *Nature*, *410*, 1049–1056, 2001.

Forte, A. M., and H. K. C. Perry, Geodynamic evidence for a chemically depleted continental tectosphere, *Science*, *290*, 1940–1944, 2000.

Fowler, A. C., Fast thermoviscous convection, *Stud. Appl. Math.*, *72*, 189–219, 1985.

Galer, S. J. G., and K. Mezger, Metamorphism denudation and sea level in the Archean and cooling of the Earth, *Precambrian Res.*, *92*, 387–412, 1998.

Gao, S., R. L. Rudnick, R. W. Carlson, W. F. McDonough, and Y. S. Liu, Re-Os evidence for replacement of ancient mantle lithosphere beneath the North China craton, *Earth Planet. Sci. Lett.*, *198*, 307–322, 2002.

Grasset, O., and E. M. Parmentier, Thermal convection in a volumetrically heated, infinite Prandtl number fluid with strongly temperature-dependent viscosity: Implications for planetary evolution, *J. Geophys. Res.*, *103*, 18,171–18,181, 1998.

Griffin, W. L., S. Y. O'Reilly, and C. G. Ryan, The composition and origin of sub-continental mantle, in *Mantle Petrology: Field Observations and High Pressure Experimentation: A Tribute to Francis R. (Joe) Boyd*, edited by Y. Fei, C. M. Bertka, and B. O. Mysen, *Spec. Publ. Geochem. Soc.*, *6*, 13–45, 1999.

Haggerty, S. E., Diamond formation and kimberlite-clan magmatism in cratonal settings, in *Mantle Petrology: Field Observations and High Pressure Experimentation: A Tribute to Francis R. (Joe) Boyd*, edited

by Y. Fei, C. M. Bertka, and B. O. Mysen, *Spec. Publ. Geochem. Soc.*, *6*, 3–12, 1999.
Haggerty, S. E., and V. Sautter, Ultradeep (greater than 300 kilometers), ultramafic upper mantle xenoliths, *Science*, *248*, 993–996, 1990.
Hanghøj, K., P. Kelemen, S. Bernstein, J. Blusztajn, and R. Frei, Osmium isotopes in the Wiedemann Fjord mantle xenoliths: A unique record of cratonic mantle formation by melt depletion in the Archaean, *Geochem. Geophys. Geosyst.*, *2*, 2000GC000085, 2001.
Herzberg, C., Phase equilibrium constraints on the formation of cratonic mantle, in *Mantle Petrology: Field Observations and High Pressure Experimentation: A Tribute to Francis R. (Joe) Boyd*, edited by Y. Fei, C. M. Bertka, and B. O. Mysen, *Spec. Publ. Geochem. Soc.*, *6*, 241–257, 1999.
Hirth, G., R. L. Evans, and A. D. Chave, Comparison of continental and oceanic mantle electrical conductivity, Is the Archean lithosphere dry?, *Geochem. Geogeophys. Geosyst.*, *1*, 2000GC000045, 2000.
Jaupart, C., and J. C. Mareschal, The thermal structure and thickness of continental roots, *Lithos*, *48*, 93–114, 1999.
Jaupart, C., J. C. Mareschal, L. Guillou-Frottier, and A. Davaille, Heat flow and thickness of the lithosphere in the Canadian Shield, *J. Geophys. Res.*, *103*, 15,269–15,286, 1998.
Jordan, T. H., Continents as a chemical boundary layer, *Philos. Trans. R. Soc. London, Ser. A*, *301*, 359–373, 1981.
Kaminski, E., and C. Jaupart, Lithospheric structure beneath the Phanerozoic intracratonal basins of North America, *Earth Planet. Sci. Lett.*, *178*, 139–149, 2000.
Kawada, Y., and S. Honda, Parameterization of heat transport by non-Newtonian convection, *Geophys. J. Int.*, *137*, 441–448, 1999.
Kukkonen, I. T., and P. Peltonen, Xenolith-controlled geotherm for the central Fennoscandian shield: Implications for lithosphere-asthenosphere relations, *Tectonophysics*, *304*, 301–315, 1999.
Lenardic, A., On the partitioning of mantle heat loss below oceans and continents over time and the relationship to the Archean paradox, *Geophys. J. Int.*, *134*, 706–720, 1998.
Lenardic, A., and L. Moresi, A new class of equilibrium geotherms in the deep thermal lithosphere of continents, *Earth Planet. Sci. Lett.*, *176*, 331–3338, 2000.
Lenardic, A., W. M. Kaula, and D. L. Bindschadler, A mechanism for crust recycling on Venus, *J. Geophys. Res.*, *98*, 18,697–18,705, 1993.
Lenardic, A., L. Moresi, and H. Mühlhaus, The role of mobile belts for the longevity of deep cratonic lithosphere: The crumple zone model, *Geophys. Res. Lett.*, *27*, 1235–1238, 2000.
Lenardic, A., L.-N. Moresi, and H. Muhlhaus, The longevity and stability of cratonic lithosphere: Insights from numerical simulations of coupled mantle convection and continental tectonics, *J. Geophys. Res.*, *108*, doi:10.1029/2002JB001859, in press, 2003.
Macdougall, J. D., and S. E. Haggerty, Ultramafic xenoliths from African kinberlites: Sr and Nd isotopic compositions suggest complex history, *Earth Planet. Sci. Lett.*, *170*, 73–82, 1999.
Moore, W. B., G. Schubert, and P. Tackley, The role of rheology in lithospheric thinning by mantle plumes, *Geophys. Res. Lett.*, *26*, 1073–1076, 1999.
Moresi, L.-N., and V. S. Solomatov, Mantle convection with a brittle lithosphere: Thoughts on the global tectonic styles of the Earth and Venus, *Geophys. J. Int.*, *133*, 669–682, 1998.
Panasyuk, S. V., and B. H. Hager, Inversion for mantle viscosity profiles constrained by dynamic topography and the geoid, and their estimated errors, *Geophys. J. Int.*, *143*, 821–826, 2000.
Pari, G., and W. R. Peltier, Global surface heat flux anomalies from seismic tomography-based models of mantle flow: Implications for mantle convection, *J. Geophys. Res.*, *103*, 23,743–23,780, 1998.
Pearson, D. G., The age of continental roots, *Lithos*, *48*, 171–194, 1999.
Pollack, H. N., Cratonization and thermal evolution of the mantle, *Earth Planet. Sci. Lett.*, *80*, 175–182, 1986.
Priestley, K., Velocity structure of the continental upper mantle: Evidence from southern Africa, *Lithos*, *48*, 45–56, 1999.
Reese, C. C., V. S. Solomatov, and L.-N. Moresi, Heat transport efficiency for stagnant lid convection with dislocation viscosity: Application to Mars and Venus, *J. Geophys. Res.*, *103*, 13,643–13,657, 1998.
Reese, C. C., V. S. Solomatov, and L.-N. Moresi, Non-Newtonian stagnant lid convection and magmatic resurfacing on Venus, *Icarus*, *139*, 67–80, 1999.
Richards, M. A., W.-S. Yang, J. R. Baumgardner, and H.-P. Bunge, Role of a low-viscosity zone in stabilizing plate tectonics: Implications for comparative terrestrial planetology, *Geochem. Geophys. Geosyst.*, *2*, 2000GC000115, 2002.
Richter, F. M., Convection and the large-scale circulation of the mantle, *J. Geophys. Res.*, *78*, 8735–8745, 1973.
Richter, F. M., A major change in the thermal state of the Earth at the Archean-Proterozoic boundary: Consequences for the nature and preservation of the Archean lithosphere, *J. Petrol., Spec. Lithosphere Issue*, 39–52, 1988.
Ritsema, J., and H. van Heist, New seismic model of the upper mantle beneath Africa, *Geology*, *28*, 63–66, 2000.
Ritsema, J., A. A. Nyblade, T. J. Owens, C. L. Langston, and J. C. VanDecar, Upper mantle seismic velocity structure beneath Tanzania, east Africa: Implications for the stability of cratonic lithosphere, *J. Geophys. Res.*, *103*, 21,201–21,213, 1998.
Röhm, A. H. E., R. Snieder, S. Goes, and J. Trampert, Thermal structure of continental upper mantle inferred from S-wave velocity and surface heat flow, *Earth Planet. Sci. Lett.*, *181*, 395–407, 2000.
Rudnick, R. L., and A. A. Nyblade, The thickness and heat production of Archean lithosphere: Constraints from xenolith thermobarometry and surface heat flow, in *Mantle Petrology: Field Observations and High Pressure Experimentation: A Tribute to Francis R. (Joe) Boyd*, edited by Y. Fei, C. M. Bertka, and B. O. Mysen, *Spec. Publ. Geochem. Soc.*, *6*, 3–12, 1999.
Saltzer, R. L., N. Chatterjee, and T. L. Grove, The spatial distribution of garnets and pyroxenes in mantle peridoties: Pressure-temperature history of peridotites from the Kaapvaal craton, *J. Petrol.*, *42*, 2229–2231, 2001.
Schmidberger, S. S., A. Simonetti, D. Francis, and C. Gariepy, Probing Archean lithosphere using the Lu-Hf isotope systematics of periodite xenoliths from Somerset Island kimberlites, Canada, *Earth Planet. Sci. Lett.*, *197*, 245–259, 2002.
Shapiro, S. S., B. H. Hager, and T. H. Jordan, The continental tectosphere and Earth's long-wavelength gravity field, *Lithos*, *48*, 135–152, 1999a.
Shapiro, S. S., B. H. Hager, and T. H. Jordan, Stability and dynamics of the continental tectosphere, *Lithos*, *48*, 115–133, 1999b.
Silver, P., D. Mainprice, W. Ben Ismïl, A. Tommasi, and G. Barruol, Mantle structural geology from seismic anisotropy, in *Mantle Petrology: Field Observations and High Pressure Experimentation: A Tribute to Francis R. (Joe) Boyd*, edited by Y. Fei, C. M. Bertka, and B. O. Mysen, *Spec. Publ. Geochem. Soc.*, *6*, 79–103, 1999.
Simons, F. J., A. Zielhuis, and R. D. van der Hilst, The deep structure of the Australian continent from surface wave tomography, *Lithos*, *48*, 17–43, 1999.
Sleep, N. H., Stress and flow beneath island arcs, *Geophys. J. R. Astron. Soc.*, *42*, 827–857, 1975.
Sleep, N. H., Gradual entrainment of a chemical layer at the base of the mantle by overlying convection, *Geophys. J.*, *95*, 437–447, 1988.
Sleep, N. H., Hotspots and mantle plumes: Some phenomenology, *J. Geophys. Res.*, *95*, 6715–6736, 1990.
Sleep, N. H., Lithospheric thinning by midplate mantle plumes and the thermal history of hot plume material ponded at lithospheric depths, *J. Geophys. Res.*, *99*, 9327–9343, 1994.
Sleep, N. H., Lateral flow and ponding of starting plume material, *J. Geophys. Res.*, *102*, 10,001–10,012, 1997.
Solomatov, V. S., Scaling of temperature- and stress-dependent viscosity convection, *Phys. Fluids*, *7*, 266–274, 1995.
Solomatov, V. S., Grain size-dependent viscosity convection and the thermal evolution of the Earth, *Earth Planet. Sci. Lett.*, *91*, 203–212, 2001.
Solomatov, V. S., and L.-N. Moresi, Three regimes of mantle convection with non-Newtonian viscosity and stagnant lid convection on the terrestrial planets, *Geophys. Res. Lett.*, *24*, 1907–1910, 1997.
Solomatov, V. S., and L.-N. Moresi, Scaling of time-dependent stagnant lid convection: Application to small-scale convection on Earth and other terrestrial planets, *J. Geophys. Res.*, *105*, 21,795–21,817, 2000.
Solomatov, V. S., and L.-N. Moresi, Small-scale convection in the D″ layer, *J. Geophys. Res.*, *107*(B1), 2016, doi:10.1029/2000JB000063, 2002.
Stacey, F. D., A thermal model of the Earth, *Phys. Earth. Planet. Inter.*, *15*, 341–348, 1977.
Stein, S., and A. Pelayo, Seismological constraints on stress in the oceanic lithosphere, *Philos. Trans. R. Soc. London, Ser. A*, *337*, 53–72, 1991.
Steinberger, B., and R. J. O'Connell, Advection of plumes in mantle flow: Implications for hotspot motion, mantle viscosity and plume distribution, *Geophys. J. Int.*, *132*, 412–434, 1998.
Tackley, P. J., Self-consistent generation of tectonic plates in time-dependent, three-dimensional mantle convection simulations: 2. Strain weakening and asthenosphere, *Geochem. Geophys. Geosystems 1*, Paper number 2000GC000043, 2000.
Turcotte, D. L., and G. Schubert, *Geodynanics: Applications of Continuum Physics to Geological Problems*, 450 pp., John Wiley, New York, 1982.
van der Lee, S., and G. Nolet, Upper mantle *S* velocity structure of North America, *J. Geophys. Res.*, *102*, 22,815–22,838, 1997.
Zoback, M. L., and M. D. Zoback, Crustal stress and intraplate deformation, *Geowissenschaften*, *15*, 116–123, 1997.

N. H. Sleep, Department of Geophysics, Stanford University, Mitchell Building, Room 640, 397 Panama Mall, Stanford, CA 94305-2215, USA. (norm@pangea.stanford.edu)